A human antibody against pathologic IAPP aggregates protects beta cells in type 2 diabetes

Fabrice Heitz
Neurimmune AG
Fabian Wirth
Neurimmune AG
Christine Seeger
Neurimmune AG
Ioana Combaluzier
Neurimmune AG
Karin Breu
Neurimmune AG
Heather Denroche
BC Children's Hospital Research Institute and Centre for Molecular Medicine and Therapeutics, Departments of Surgery and Pathology & Laboratory Medicine, University of British Columbia https://orcid.org/0000-0002-0976-2656
Julien Thevenet
Univ. Lille, Inserm, CHU Lille, U1190 - EGID https://orcid.org/0000-0001-6873-8640
Melania Osto
Institute of Veterinary Physiology, Vetsuisse Faculty of the University of Zürich
Paolo Arosio
Institute for Chemical and Bioengineering, ETH Zürich
Julie Kerr-Conte
Inserm
C. Verchere
BC Children's Hospital Research Institute and Centre for Molecular Medicine and Therapeutics, Departments of Surgery and Pathology & Laboratory Medicine, University of British Columbia
François Pattou
Inserm U1190
Thomas Lutz
University of Zurich
Marc Donath
University Hospital of Basel https://orcid.org/0000-0002-3143-5045
Christoph Hock
Neurimmune

Roger Nitsch
Neurimmune
Jan Grimm (jan.grimm@neurimmune.com)
Neurimmune https://orcid.org/0000-0002-3898-3298

Article

Keywords: type 2 diabetes, IAPP, amylin, islet amyloid, immunotherapy, beta cells

Posted Date: February 2nd, 2021

DOI: https://doi.org/10.21203/rs.3.rs-147509/v1

Version of Record: A version of this preprint was published at Nature Communications on October 9th, 2023. See the published version at https://doi.org/10.1038/s41467-023-41986-0.

Abstract

In patients with type 2 diabetes, pancreatic beta cells progressively degenerate and gradually lose their ability to produce insulin and regulate blood glucose. Beta cell dysfunction and loss is associated with an accumulation of aggregated forms of islet amyloid polypeptide (IAPP) consisting of soluble prefibrillar IAPP oligomers as well as insoluble IAPP fibrils in pancreatic islets. Here, we describe a novel human monoclonal antibody selectively targeting IAPP oligomers and neutralizing IAPP aggregate toxicity by preventing membrane disruption and apoptosis *in vitro*. Antibody treatment in rats and mice transgenic for human IAPP, and human islet-engrafted mouse models of type 2 diabetes triggered clearance of IAPP oligomers resulting in beta cell protection and improved glucose control. These results provide new evidence for the pathological role of IAPP oligomers and suggest that antibody-mediated removal of IAPP oligomers could be a pharmaceutical strategy to support beta cell function in type 2 diabetes.

Introduction

Type 2 diabetes (T2D) is a chronic metabolic disorder characterized by insulin resistance and progressive dysfunction and loss of insulin-producing pancreatic beta cells, resulting in insulin deficiency and elevated blood glucose. Beta cell death is accompanied by the accumulation and aggregation of the 37-residue peptide hormone islet amyloid polypeptide (IAPP or amylin) that is co-secreted with insulin and forms amyloid deposits in a majority of pancreatic islets from T2D patients[1]. In its physiological monomeric conformation, IAPP acts as a regulator of glucose homeostasis through satiety control and inhibition of gastric emptying[2,3]. As IAPP is highly amyloidogenic under conditions of increased secretory demand it can readily misfold and aggregate into soluble oligomers and insoluble amyloid fibrils that are thought to contribute to beta cell dysfunction and death in T2D[4–6]. The involvement of IAPP aggregates in beta cell decline and T2D progression is supported by an increasing body of evidence. First, amyloid severity inversely correlates with beta cell area in pancreatic islets of T2D patients[4]. Second, a sporadic mutation in the human *IAPP* coding sequence leading to a S20G amino acid substitution is associated with a higher peptide propensity for aggregation, an increased risk for developing T2D and a more severe form of the disease[7–9]. Third, cat and primates producing amyloidogenic variants of IAPP and forming pancreatic islet amyloid deposits naturally develop signs of T2D[10]. In non-human primates, islet amyloid severity was also shown to correlate with beta cell loss and T2D progression[11,12]. Fourth, while rodent IAPP is unable to aggregate into amyloid, transgenic mice and rats expressing human IAPP (hIAPP) spontaneously develop a T2D phenotype characterized by islet amyloidosis and decreased beta cell mass[13–16]. Likewise, humanization of the non-amyloidogenic porcine IAPP using CRISPR/Cas9 gene editing leads to T2D in miniature pigs[17]. Of note, IAPP aggregation is also linked to beta cell deterioration in human islets cultured in high glucose or transplanted into mice or humans with type 1 diabetes[18–20]. Synthetic IAPP aggregates, primarily oligomers produced at an early stage of amyloid fibril formation, induce beta cell dysfunction and apoptosis *in vitro*[21]. Their cytotoxicity presumably results from membrane permeabilization[22,23], induction of oxidative and ER stress[24,25], and pro-inflammatory cytokine

release[26,27]. However, the contribution of IAPP oligomers to beta cell loss and T2D progression remains controversial and has not been yet clearly established *in vivo*. Monoclonal antibodies are approved therapeutic agents that offer the unique advantage of neutralizing and facilitating the removal of specific disease-related target antigens. We hypothesized that accumulation of IAPP oligomers in pancreatic islets is responsible for dysfunction and degeneration of beta cells observed in T2D, and that passive immunization with monoclonal antibodies directed against IAPP oligomers may protect beta cells and provide therapeutic efficacy. To this end, we developed a human monoclonal antibody highly selective for toxic IAPP oligomer species that was evaluated for its ability to clear IAPP oligomers, preserve beta cell function and prevent disease progression in rodent models of T2D.

Results

A human monoclonal antibody with high affinity and selectively for aggregated hIAPP.

We identified and recombinantly cloned a monoclonal antibody of IgG1 subclass (termed α-IAPP-O) selectively targeting pathologic human IAPP (hIAPP) aggregates by analyses of complements of human memory B cells derived from a clinically selected human population composed of healthy elderly donors. The α-IAPP-O antibody selectively immunoreacted at a low nanomolar concentration with extracellular hIAPP aggregates present on amyloid-positive pancreatic islets from type 2 diabetic subjects (**Fig. 1a**,**b**), with absence of binding to native physiological hIAPP monomers within insulin-producing pancreatic beta cells and to unrelated disease-associated amyloidogenic proteins and β-amyloid plaques in the brain of Alzheimer's disease patients (**Supplementary Fig. 1**). α-IAPP-O binding kinetics revealed high affinity for hIAPP aggregates (K_D=1.54 nM) likely consisting of a heterogenous mixture of aggregated species, as compared to monomeric hIAPP (biotin-hIAPP, K_D=2.84 μM) using biolayer interferometry (**Fig. 1c**,**d** and **Supplementary Table 1**). Binding affinity of the monovalent α-IAPP-O Fab fragment to hIAPP aggregates (K_D=6.47 μM) was 4000-fold lower compared to the bivalent IgG1 format (**Fig. 1e** and **Supplementary Table 1**), suggesting a strong avidity component in α-IAPP-O binding to epitope-rich hIAPP aggregates. The α-IAPP-O epitope was mapped to an N-terminal sequence conserved among hIAPP and less amyloidogenic IAPP orthologues and binding was impaired by proline substitution in the amyloidogenic region responsible for amyloid fibril formation, C-terminal truncation and SDS-induced denaturation (**Supplementary Fig. 2**).

α-IAPP-O preferentially binds to hIAPP prefibrillar oligomers.

Human IAPP rapidly aggregated into amyloid fibrils visualized by transmission electron microscopy, and amyloid growth monitored by thioflavin-T (ThioT) fluorescence followed a sigmoidal kinetics characterized by a short lag phase, an exponential growth phase and an equilibrium phase (**Fig. 2a**). To elucidate the nature of aggregated hIAPP species recognized by α-IAPP-O, we performed time-resolved

immunoblot analysis of fractions collected over the course of amyloid fibril formation. α-IAPP-O was shown to preferentially immunoreact with transient prefibrillar oligomers that are produced during the lag and the growth phases of amyloid formation (**Fig. 2b**). In contrast to a non-selective IAPP antibody (α-IAPP), α-IAPP-O bound neither to monomeric hIAPP nor to non-amyloidogenic rodent IAPP (rIAPP) and detergent-denatured hIAPP aggregates. α-IAPP-O recognized high molecular weight hIAPP species (>200 kDa) but not monomers or chemically cross-linked aggregates generated *in vitro* and resolved by non-reducing SDS-PAGE and Western blotting (**Fig. 2c**). We next studied the effect of α-IAPP-O on hIAPP aggregation using kinetic modelling of molecular events underlying amyloid fibril formation[28–32]. Aggregation kinetics of hIAPP, unseeded or seeded by adding preformed fibrillar hIAPP, were compatible with models describing either fragmentation or secondary nucleation-dominated mechanisms (**Supplementary Fig. 3**). In both cases, model analysis indicates that α-IAPP-O concentration-dependently delayed fibril formation by inhibiting primary nucleation, with minimal effects on fibril-dependent processes such as elongation, secondary nucleation and fragmentation (**Fig. 2d**,**e** and **Supplementary Fig. 4** and **5**). This was further confirmed by experiments performed after pre-incubating seeds with α-IAPP-O (**Fig. 2f**). Consistent with selective inhibition of primary nucleation, a higher substoichiometric concentration of α-IAPP-O (10 hIAPP: 1 α-IAPP-O ratio) fully inhibited the formation of amyloid fibrils (**Fig. 2g**) by complexing pre-fibrillar oligomers with sizes ranging from 60 to 500 nm (**Fig. 2h** and **Supplementary Fig. 6**). Taken together, these data indicate that α-IAPP-O selectively targets hIAPP oligomers produced at an early stage of the aggregation process (**Supplementary Figure 5e**).

α-IAPP-O prevents membrane deposition of hIAPP oligomers and beta cell apoptosis.

Incubation of beta cells with hIAPP oligomers formed *in vitro* reduced the viability by 95% and increased apoptosis identified by TUNEL staining to 85% (**Fig. 3a**,**b**). Cytotoxicity was not observed when applying amyloid fibrils (**Supplementary Fig. 7a**,**b**). α-IAPP-O neutralized cytotoxicity and apoptosis in a concentration-dependent manner as compared to an IgG control antibody. Beta cell apoptosis was accompanied by cell membrane deposition of hIAPP oligomers and ThioS-positive amyloid fibrils (**Fig. 3c-e** and **Supplementary Fig. 7c**,**d**). α-IAPP-O concentration-dependently inhibited the deposition of hIAPP on INS-1 beta cells (**Fig. 3e** and **Supplementary Fig. 7d**) and prevented permeabilization of liposome membranes induced by hIAPP oligomers (**Fig. 3f**,**g**). We next determined the effects of α-IAPP-O on human islets isolated from obese donors at risk for diabetes (**Supplementary Table 2**). Human islets were exposed to high glucose leading to the accumulation of extracellular ThioS-positive amyloid deposits and to beta cell apoptosis (**Fig. 3h**). Co-incubation with α-IAPP-O (0.5 μM) reduced ThioS-positive amyloid load and apoptotic beta cell death compared to IgG control. Further, α-IAPP-O improved beta cell function

evaluated by insulin response to elevated glucose using islet perifusion, similar to the amyloid-inhibiting compound Congo red[33] at high concentration (25 µM) (**Fig. 3i** and **Supplementary Fig. 7e**).

α-IAPP-O improves key pathological features of type-2 diabetes in rats and mice.

The effects of α-IAPP-O were next evaluated in a transgenic rat model with beta cell-specific expression of hIAPP. Transgenic rats were shown to spontaneously develop a diabetic phenotype characterized by extensive islet amyloid formation resulting in progressive beta cell dysfunction and loss, ultimately leading to insulin depletion and hyperglycemia[15,16]. In this model, α-IAPP-O specifically engaged extracellular hIAPP oligomers surrounding insulin-producing beta cells in transgenic rat islets (**Fig. 4a)**. The antibody did not bind to extracellular ThioS-positive amyloid, nor to monomeric IAPP constitutively expressed within transgenic and wild-type beta cells (**Fig. 4a** and **Supplementary Fig. 8**). Pre-diabetic transgenic rats characterized by emerging glucose intolerance (**Supplementary Fig. 9a**) were weekly administered with the rat chimeric analogue of α-IAPP-O (^{ch}α-IAPP-O, 3 mg/kg i.p.). ^{ch}α-IAPP-O reduced the progression of glucose intolerance and improved glucose-stimulated insulin secretion compared to vehicle after 8, 15 and 24 weeks of treatment with steady state plasma drug titers around 90 µg/ml (**Fig. 4b**,**c** and **Supplementary Fig. 9a**,**b**). The glucose-lowering drug metformin[34,35] (200 mg/kg/day in drinking water) improved glucose tolerance to a similar degree as did ^{ch}α-IAPP-O but failed to stimulate insulin secretion upon oral glucose challenge. The combination of ^{ch}α-IAPP-O and metformin had no cumulative effect on glucose control but ameliorated insulin secretion similarly to ^{ch}α-IAPP-O monotherapy, indicating a direct protective effect of ^{ch}α-IAPP-O on beta cell function (**Supplementary Fig. 9c**). ^{ch}α-IAPP-O efficacy was target-related as it had no glucose-lowering effect in wild-type rats, and an isotype control antibody had no impact on glycemia in transgenic or wild-type rats (**Supplementary Fig. 9d**). In a separate study, rats with marked glucose intolerance and hyperglycemia at baseline (**Supplementary Fig. 10a**,**b**) received weekly dosing of ^{ch}α-IAPP-O (1, 3 and 10 mg/kg i.p.). ^{ch}α-IAPP-O treatment was associated with significant improvements in glucose tolerance, glucose-stimulated insulin response and beta cell function at 1 and 10 mg/kg compared to vehicle (**Fig. 4d-f** and **Supplementary Fig. 10c**). These effects were accompanied by reduced glycemia, increased circulating insulin levels and normalized body weight (**Fig. 4g-i** and **Supplementary Fig. 10d**). ^{ch}α-IAPP-O treatment was already effective after 7 weeks and effects became more apparent as the phenotype progressed (**Supplementary Fig. 10e**,**f**). Slowing of disease progression was associated with preserved islet size and beta cell content in the pancreas of rats treated with ^{ch}α-IAPP-O relative to vehicle (**Fig. 4j**,**k** and **Supplementary Fig. 10g**). ^{ch}α-IAPP-O treatment was also associated with an increase in soluble IAPP levels and a decrease in insoluble IAPP aggregates in pancreas homogenates (**Fig. 4l**). Further, we confirmed the therapeutic effects of α-IAPP-O in hIAPP transgenic mice characterized by glucose intolerance, hyperglycemia and insulin deficiency together with islet amyloidosis, oligomer deposition and beta cell loss (**Supplementary Fig. 11**). In this independent

model, weekly administration of mouse chimeric ^{ch}α-IAPP-O (10 mg/kg i.p.) but not an isotype-matched control antibody improved glycemia and protected pancreatic beta cells (**Supplementary Fig. 11b-h**).

α-IAPP-O removes extracellular hIAPP oligomers in transgenic rat islets.

We further investigated the mechanism of action of α-IAPP-O in transgenic rats comparing ^{ch}α-IAPP-O to an immunologically inert variant (inert ^{ch}α-IAPP-O) carrying a mutated Fc region eliminating the interaction to rat Fc gamma receptors and silencing effector functions (**Supplementary Fig. 12**). Pre-diabetic rats were dosed once a week with ^{ch}α-IAPP-O (1, 3 and 10 mg/kg i.p.) and inert ^{ch}α-IAPP-O (10 mg/kg i.p). ^{ch}α-IAPP-O dose-dependently reduced immunoreactive hIAPP oligomers by up to 68% relative to vehicle without significantly affecting ThioS-positive amyloid deposition in transgenic rat islets (**Fig. 5a**,**b** and **Supplementary Fig. 13a**,**b**). Likewise, ^{ch}α-IAPP-O decreased total pancreatic IAPP aggregates measured by ELISA (**Supplementary Fig. 13c**). Oligomer removal was paralleled by recruitment of CD68-positive islet resident macrophages to hIAPP oligomers and fibrils, without affecting the total number of islet macrophages (**Fig. 5c** and **Supplementary Fig. 13d**). In addition, clearance of hIAPP oligomers was associated with increased insulin-immunoreactive beta cell area and reduced levels of the disease-relevant pro-inflammatory cytokine IL-1β[26,27] in the pancreas (**Fig. 5d** and **Supplementary Fig. 13e**,**f**). In contrast, inert ^{ch}α-IAPP-O did neither significantly affect hIAPP oligomer deposition, macrophage recruitment and IL-1β levels, nor preserve beta cell content despite a small reduction in islet amyloid load (**Fig. 5a-d** and **Supplementary Fig. 13a-f**). Consistent with these findings and with the involvement of hIAPP oligomers in macrophage-mediated inflammation[26,36], α-IAPP-O dose-dependently stimulated Fc gamma receptor-mediated phagocytosis of hIAPP oligomers, and to a lesser extent of hIAPP fibrils, by human PBMC- and THP-1-derived macrophages *in vitro*, while decreasing macrophage IL-1β release (**Fig. 5e** and **Supplementary Fig. 14**).

α-IAPP-O prevents diabetes in human islet-engrafted mouse models.

IAPP aggregation and amyloid deposition has been reported in transplanted human pancreatic islets where it might contribute to graft failure and recurrence of hyperglycemia[37–39]. To evaluate the effect of α-IAPP-O on graft function *in vivo*, immunodeficient NSG mice rendered diabetic by streptozotocin (STZ) injection or Rag2$^{-/-}$ mice fed a high-fat diet (HFD)[38,40] were both transplanted with human islets from non-diabetic and pre-diabetic donors (**Fig. 6a** and **Supplementary Table 2**). While NSG recipient mice weekly

administered with ^{ch}IgG (10 mg/kg i.p.) rapidly returned to hyperglycemia, ^{ch}α-IAPP-O (10 mg/kg i.p.) treatment maintained normoglycemia and delayed the recurrence of diabetes (**Fig. 6b**,**c** and **Supplementary Fig. 15a**). Human islet-engrafted Rag2$^{-/-}$ mice fed a HFD two weeks post-transplant for twelve weeks developed glucose intolerance, hyperglycemia and hyperinsulinemia accompanying obesity, as opposed to non-obese recipients fed a control diet (**Fig. 6d**-**g**). Treatment with ^{ch}α-IAPP-O (10 mg/kg i.p., once weekly) along with HFD normalized glycemia, and consistently reduced plasma insulin and human C-peptide levels (**Fig. 6d**-**f** and **Supplementary Fig. 15b**,**c**), pointing towards an improved function and adaptation of engrafted human islets. Furthermore, ^{ch}α-IAPP-O treatment (10 mg/kg i.p., once weekly) initiated in obese diabetic mice previously fed a HFD for six weeks reversed abnormal glucose tolerance, while glucose tolerance deteriorated because of graft dysfunction in recipients receiving ^{ch}IgG (10 mg/kg i.p., once weekly) (**Fig. 6h** and **Supplementary Fig. 15d**). Graft analysis revealed a high number of infiltrating macrophages associated with a decrease in oligomeric hIAPP but not amyloid deposits upon ^{ch}α-IAPP-O treatment (**Fig. 6i**), in line with stimulation of macrophage-mediated phagocytic clearance of toxic hIAPP oligomers.

Discussion

Clinically, the progressive nature of T2D is linked to beta cell dysfunction and loss, with patients lacking the ability to produce sufficient endogenous insulin to counteract insulin resistance and to control blood glucose levels[41]. While the primary cause of beta cell failure in T2D is unknown, the accumulation of aggregated forms of the beta cell peptide hormone hIAPP in pancreatic islets is a likely contributor to decreased beta cell function and mass in an early stage of the disease. We describe here that hIAPP oligomers can cause beta cell dysfunction and death during T2D development which can be prevented by applying a human-derived antibody selective for these toxic hIAPP species in cultured beta cells and isolated human islets, as well as in transgenic rodents and human islet-engrafted mouse models.

The data provide evidence that hIAPP prefibrillar oligomers applied to beta cells induce apoptosis *in vitro*, in contrast to monomers and mature fibrils. Neutralization of hIAPP oligomers by α-IAPP-O, a human monoclonal IgG1 antibody selectively binding extracellular hIAPP deposits in the pancreas of T2D patients and hIAPP intermediates produced during amyloid formation, prevented cell accumulation of amyloid fibrils, lipid membrane disruption and beta cell toxicity. This is in line with previous studies indicating that toxic hIAPP oligomers deposit at the cell surface and permeabilize the cell membrane via pore formation and/or elongation into amyloid fibrils[42]. We have also shown that α-IAPP-O interacts with the N-terminus of IAPP when self-assembled into oligomers and inhibits the formation of amyloid fibril end-product, supporting a key role of IAPP N-terminal residues in the initial aggregation process facilitating membrane interaction and permeation[43]. Treatment with α-IAPP-O and with a general inhibitor of aggregation reduced islet amyloid content and beta cell toxicity in isolated human islets exposed to elevated glucose levels, strengthening the role of hIAPP oligomers and islet amyloidosis in human beta cell deterioration under diabetic conditions such as hyperglycemia. Of note, beta cell toxicity solely caused by hIAPP aggregates and independently of hyperglycemia was also reported in human and

hIAPP-expressing mouse islets[44,45]. In these studies, beta cell apoptosis has been associated with oxidative stress, Fas upregulation and caspase-8 activation. Additional mechanisms by which hIAPP aggregates could mediate islet beta cell apoptosis and that are characteristic of human T2D include membrane disruption[46], endoplasmic reticulum (ER) stress[24], defects in autophagy[47], activation of the receptor for advanced glycation end-products (RAGE)[48] and inflammation[26,27,36]. These pathways potentially contribute to hIAPP-induced beta cell loss and development of diabetes. This has been extensively studied in hIAPP-expressing transgenic rats and mice recapitulating features of human T2D[13–16]. In these animal models, both intracellular and extracellular hIAPP oligomers have been reported to trigger beta cell dysfunction and loss. Our data support a direct role for extracellular oligomers in beta cell pathogenesis, diabetes onset and progression *in vivo*. First, we have demonstrated that α-IAPP-O selectively engages extracellular oligomers in overtly diabetic hIAPP transgenic rats and mice after a single intraperitoneal injection. Oligomers bound by α-IAPP-O were extensively deposited around islet beta cells with a distribution distinct from amyloid fibrils. Second, chronic administration of α-IAPP-O in prediabetic and diabetic transgenic animals reduced beta cell loss and improved insulin secretion and glycemia. α-IAPP-O also prevented beta cell failure and diabetes development in human islet-engrafted mice, ruling out any confounding effects of hIAPP expression in transgenic models.

The mechanism of action of α-IAPP-O was dependent on the phagocytic clearance of extracellular hIAPP oligomers, but not amyloid, by islet macrophages *in vivo*. Although macrophages were recruited at sites of amyloid deposition, we did not observe any effect on amyloid load, consistent with the selective binding of α-IAPP-O toward hIAPP oligomers but not amyloid fibrils. Other possible explanations are the limited capacity of macrophages to degrade and clear islet amyloid fibrils[49] and the constant buildup of amyloid fibrils in islets with a high functional beta cell mass[50].

Together, our findings indicate that antibody-mediated removal of extracellular hIAPP oligomers in an early phase of events leading to beta cell exhaustion can preserve beta cell function and limit the progression of T2D. This is of particular relevance since the effectiveness of currently available treatments for T2D are limited in time and likely impacted by the continuous deterioration of beta cell function over the course of the disease[51]. Novel treatment strategies to delay disease progression by restoring and durably preserving beta cell function are needed[52,53]. Anti-diabetic medications offering blood glucose control by improving peripheral insulin sensitivity such as metformin, or by increasing insulin secretion such as dipeptidyl peptidase-4 (DPP-4) inhibitors and glucagon-like peptide-1 receptor agonists (GLP-1 RAs) have demonstrated benefits in beta cell adaptation to high-fat diet-induced insulin resistance in hIAPP transgenic rodents and short-term improvements in human islet graft function in diabetic mouse recipients[34,54–56]. However, evidence for a long-term impact of these drugs on the progressive deterioration of beta cell function are lacking[57–60].

The therapeutic development of evolutionarily optimized human antibodies directed against misfolded and aggregated endogenous proteins delivered promising preclinical and clinical findings in degenerative brain diseases such as Alzheimer's disease[61], Parkinson's disease[62], amyotrophic lateral sclerosis (ALS)

and fronto-temporal dementia (FTD)[63,64]. Our data with the human-derived antibody α-IAPP-O targeting toxic IAPP oligomers expand this therapeutic concept towards T2D and opens a new avenue for beta cell protective therapies.

Online Methods

Antibody generation

Antibodies were generated from a de-identified blood lymphocyte library collected from healthy elderly subjects by screening for high affinity binding toward aggregated IAPP and absence of cross-reactivity toward unrelated amyloid-forming proteins[61]. Antibody sequences were cloned from corresponding memory B cells using cDNA cloning of IgG heavy and kappa or lambda light chain variable region sequences, and sub-cloned into human IgG1 expression constructs using Ig framework-specific primers for human variable heavy and light chain families in combination with human J-H segment-specific primers. Chimeric analogs (^{ch}α-IAPP-O and ^{ch}α-IAPP-O/F) were engineered to contain mouse IgG2a or rat IgG2b backbones. Recombinant antibodies were expressed in CHO-S cells and purified by protein A or protein G affinity chromatography. Fab fragments were generated by enzymatic digestion of human IgG1 antibody followed by purification on an IgG-CH1 affinity column (GingisKHAN Fab kit, Genovis). The study was approved by the local ethics committee, written informed consent was obtained prior to the investigations.

Preparation of IAPP peptides

Synthetic human IAPP (hIAPP), biotinylated hIAPP (biotin-hIAPP) and rodent IAPP (rIAPP) peptides (Bachem, Switzerland) were resuspended at 2 mg/mL in pure hexafluoro-isopropanol (HFIP, Sigma) with shaking overnight at room temperature, lyophilized using an Alpha 1-2 LDplus freeze dryer (Christ), and reconstituted in buffer to the desired concentration.

Biolayer interferometry

Antibody binding kinetic was measured with an Octet RED96 instrument (Pall ForteBio). Lyophilized hIAPP was reconstituted in carbonate buffer (100 mM, pH 9.6) at 20 µg/mL or in acetate buffer (10 mM, pH 6) at 10 µg/mL and loaded on pre-equilibrated aminopropylsilane (APS) or activated amine-reactive (AR2G) biosensors (Pall ForteBio) according to manufacturer's recommendations. Biotin-hIAPP was reconstituted in kinetics buffer (Pall ForteBio) at 20 µg/mL and loaded on streptavidin (SA) biosensors. α-IAPP-O full IgG and Fab fragment were tested at indicated concentrations in PBS (pH 7.4) or kinetics buffer. Binding response relative to PBS, isotype control IgG or Fab was analyzed with simultaneous

Ka/Kd global fitting (2:1 or 1:1 interaction models) using the Octet system software. BLI sensorgrams were drawn using Prism7 software from GraphPad (San Diego, USA).

Aggregation assay and kinetic analysis

Spontaneous aggregation of hIAPP, biotin-hIAPP and rIAPP peptides (Bachem) in the absence and presence of different concentrations of antibodies was assessed by monitoring amyloid fibril formation via the increase of fluorescence of the amyloid-specific dye thioflavin-T (ThioT, Sigma) over time. Lyophilized monomeric IAPP was reconstituted at 5 and 20 µM in serum-free RPMI 1640 medium (11879-RPMI, ThermoFisher Scientific). Reconstituted peptides were mixed with ThioT (5 mM in H_2O, filtered at 0.22 µm) to a final concentration of 20 µM in 96-well clear-bottom non-binding plates (Costar), and amyloid formation was recorded on a Varioskan LUX plate reader (ThermoFisher Scientific) measuring fluorescence emission at 489 nm (excitation at 456 nm; 12 nm bandwidth) every 3 min at room temperature (while shaking at 300 rpm for 10 sec) or at a single time point corresponding to maximal fibril formation. Experimental data were analysed and fractional fibrillar mass concentration and rate constants were calculated using the AmyloFit platform[65]. Microscopic events underlying hIAPP fibril formation that are inhibited by antibodies were identified by comparing rate constants obtained in the absence and presence of antibodies in unseeded and seeded reactions.

Transmission electron microscopy

Samples were adsorbed onto glow-discharged carbon-coated copper grids (S162-3, Plano). Grids were stained with 2% (w/v) uranyl acetate for 1 min, washed with ddH_2O, air-dried and imaged using a Philips CM100 transmission electron microscope with an acceleration voltage of 80 to 100 kV.

Dot blot assay

Samples were diluted (1:3) in serum-free RPMI 1640 medium (11879-RPMI, ThermoFisher Scientific) ± 0.1% SDS and filtered through a nitrocellulose membrane (0.1 µm pore size). The membrane was washed in PBS, air-dried, blocked with PBS + 0.1% Tween® 20 (Sigma) + 5% BSA (Sigma) for 1h, and incubated with α-IAPP-O (5 µg/ml) and a rabbit anti-IAPP primary antibody (α-IAPP, 2 µg/ml; T-4145, Peninsula Laboratories) in blocking buffer for 1h at room temperature. After washing, the membrane was incubated with HRP-conjugated donkey anti-human and goat anti-rabbit secondary antibodies (1:10000; Jackson ImmunoResearch), and revealed with luminescent HRP substrate (Pierce™ ECL, ThermoFisher Scientific) using an ImageQuant LAS 4000 (GE Healthcare).

Western blotting

Lyophilized hIAPP was reconstituted at 20 µM in serum-free RPMI 1640 medium (11879-RPMI, ThermoFisher Scientific) and mixed with glutaraldehyde (0, 0.5 or 1%; G6257, Sigma), incubated at 37°C for 30 min with shaking, neutralized with 100 nM Tris-HCl pH 8 (2:1) and resolved under non-reducing and denaturing conditions by gradient SDS-PAGE (NuPAGE 4-12% Bis-Tris gels, Life Technologies) using NuPAGE LDS sample buffer (without reducing agent; Life Technologies) and NuPAGE MES running buffer (Life Technologies). Resolved proteins were electroblotted (Novex® Semi-Dry Blotter, 5V, 1 h) onto PVDF membrane. Non-specific binding sites were blocked with PBS + 0.1% Tween® 20 (Sigma) + 2% BSA (Sigma) for 1h. Membrane was immunoblotted with mouse chimeric ^{ch}α-IAPP-O (10 µg/ml) and rabbit anti-IAPP antibody (α-IAPP, 1:500; T-4157, Peninsula Laboratories International) in blocking buffer for 1h at room temperature, washed in PBS + 0.1% Tween® 20, and incubated with anti-mouse and anti-rabbit IgG (H+L) secondary antibodies coupled to HRP (1:10’000; Jackson ImmunoResearch Laboratories). Antibody binding was revealed with HRP substrate (Pierce^{TM} ECL, ThermoFisher Scientific) and imaged using an ImageQuant LAS 4000 system (GE Healthcare, Switzerland).

Dynamic light scattering

The average size of particles present in samples was measured by dynamic light scattering (DLS) at a fixed angle of θ=173 ° and a laser source of 633 nm on a Zetasizer Nano (Malvern, UK). Additionally, samples were centrifuged at 10’000 g for 15 min and supernatants (soluble fractions) were analyzed. Samples were measured in triplicates in micro UV-Cuvettes with dimension 12.5×12.5×45 mm (60 µl) and light path 1 cm (Brand GmbH, Germany).

INS-1 cells and cell-based assays

Rat insulinoma INS-1 beta cells (CRL-2058, Thermo Fisher Scientific) were grown in RPMI-1640 medium (30-2001, ATCC) supplemented with 10% fetal bovine serum (FBS), 100 µg/ml penicillin and 100 µg/ml streptomycin. Cultured cells were maintained in a humidified atmosphere of 5% CO_2 at 37°C. Cells were seeded in 96-well plates (100 µl/well; ~60% confluency) 24h prior incubation with hIAPP. Lyophilized hIAPP was reconstituted at 20 µM in serum-free RPMI 1640 medium (11879-RPMI, ThermoFisher Scientific) supplemented with 100 µg/ml penicillin and 100 µg/ml streptomycin. Human α-IAPP-O or IgG control antibody were added at indicated concentrations and peptide solutions were incubated for 4h at room temperature under quiescent conditions before being applied to INS-1 β-cells. Control cells were incubated in peptide-free culture medium.

Cell viability and apoptosis were assessed after 16h. Cell viability was evaluated using MTT assay (MTT Cell growth Assay Kit, Merck Millipore) according to manufacturer’s instructions with absorbance

measured at 570 nm using a Varioskan LUX plate reader (ThermoFisher Scientific). Cell apoptosis was visualized by TUNEL staining (In Situ Cell Death Detection Kit, TMR red; Roche). Briefly, cells were fixed in 4% paraformaldehyde for 10 min at room temperature, washed in PBS, permeabilized in 0.25% Triton X-100 (in PBS) for 10 min and blocked with a solution containing 5% serum (horse/goat) + 4% BSA in PBS for 1h, incubated with TUNEL solution (1:2 dilution; 50 µl/well) for 1h at 37°C, washed and kept in PBS for imaging. IAPP aggregates were stained on living cells exposed to human α-IAPP-O (200 nM) for 1h prior to fixation and detected using Cy2-conjugated donkey anti-human secondary antibody (1:250; Jackson Immunoresearch).

Amyloid deposition was evaluated after 12h by applying 0.01% thioflavin-S (ThioS, Sigma) in H_2O for 10 min at room temperature on fixed cells, with subsequent rinsing in ethanol 70% and H_2O. DAPI (1:1000) was included in the last washing step prior imaging.

Fluorescence images were captured using a confocal laser scanning microscope (Leica SP8) and a widefield fluorescence imaging system (IN Cell Analyzer 2500 HS, GE Healthcare). Image analysis was performed on at least 3 different fields of view per well and 3 wells per condition using Image J software. Apoptosis was counted as the number of TUNEL and DAPI double-positive nuclei relative to total number of DAPI-positive nuclei and expressed as percentage. Amyloid deposition was computed as the image area occupied by ThioS staining expressed as percentage, with 100% corresponding to cells exposed to 20 µM hIAPP in absence of antibody.

Membrane-bound IAPP aggregates were immunoprecipitated upon INS-1 cell exposure to hIAPP and rIAPP for 2h. Cells were rinsed in culture medium, gently scraped off the bottom of the wells and lysed by sonication. Cell lysates were incubated with mouse chimeric ^{ch}α-IAPP-O (20 µg/ml) or ^{ch}IgG control antibody (20 µg/ml) for 30 min at room temperature before addition of protein A-coated magnetic beads (Dynabeads, Life Technologies) for another 30 min at room temperature. After washing, antibody-antigen complexes were eluted from the beads in LDS sample buffer (Life Technologies) supplemented with 2.5 % β-mercaptoethanol (Sigma) by heating at 70°C for 10 min and resolved by Western blotting.

Membrane leakage assay

Liposomes (POPC/POPS at 7:3 molar ratio) encapsulated with 70 mM calcein disodium and formulated in 10 mM Tris–HCl, 100 mM NaCl (pH 7.4) were purchased from FormuMax Scientific Inc. (Sunnyvale, CA, USA). Leakage assay was performed in a 96-well clear bottom non-binding plate (Costar) in a total volume of 200 µL, consisting of 12 µL liposomes (0.4 mM), 8 µL of antibody in PBS at indicated concentrations, and 180 µL hIAPP (10 µM) in 10 mM Tris–HCl, 100 mM NaCl. PBS was used as control in absence of peptide and antibody. Calcein leakage was measured on a Varioskan LUX plate reader (ThermoFisher Scientific) by fluorescence emitted at 517 nm (495 nm excitation) every 3 minutes after plate was shaken for 9 sec at 400 rpm. At the end of the experiment, maximum fluorescence leakage was induced by addition of 1 µL 10% Triton-X100 (Sigma). Percentage membrane leakage was calculated by

the equation $(F-F_0)/(F_{max}-F_0)x100$, with F corresponding to fluorescence measured over time, F_0 to initial fluorescence, and F_{max} to maximum fluorescence.

Human islet culture

Human pancreas tissue was harvested from three obese adult brain-dead donors at the Centre Hospitalier Régional Universitaire de Lille (France) and islets were isolated as previously described[66]. Donor characteristics and islet information are provided in **Supplementary Table 2**. Procedures were approved in agreement with French regulations, institutional ethical committee of the University of Lille and the Centre Hospitalier Régional Universitaire de Lille. Islets were cultured in 11 mM glucose-containing CMRL media (supplemented with 100 U/mL penicillin and 100 µg/mL streptomycin) in the presence of human α-IAPP-O (0.5 µM), IgG control antibody (0.5 µM), or Congo Red (25 µM) for seven days.

Islet function was evaluated using dynamic perifusion[67]. Briefly, 500 islets were perifused (1 ml/min) with 3 mM glucose for 60 min (last 10 min used as baseline) and glucose-stimulated insulin secretion dynamics was determined at 15 mM glucose over 40 min. Insulin secretion was measured by chemiluminescent immunoassay (Access Ultrasensitive Insulin, Beckman Coulter) and calculated as insulin secretion (µUI/ml) per minute. Intra-islet insulin content is reported in **Supplementary Figure 7e**.

Cultured islets were fixed in 4% (w/v) paraformaldehyde, paraffin-embedded and cut in 3-µm sections for histological assessment of beta cell apoptosis and amyloid deposition. Sections were deparaffinized and rehydrated, permeabilized in 0.25% Triton X-100 (in PBS) for 10 min, blocked with a solution containing 5% serum (horse/goat) + 4% BSA in PBS for 1h at room temperature, incubated with TUNEL solution (1:2 dilution; In Situ Cell Death Detection Kit, TMR red; Roche) for 1h at 37°C and with 0.15% (w/v) thioflavin-S (ThioS, Sigma) in H_2O for 10 min, followed by rinsing in ethanol 70% and H_2O. DAPI (1:1000) was included in the last washing step prior slide mounting using Hydromount media (National Diagnostics). Slides were imaged on a Leica SP8 confocal laser scanning microscope. Image analysis was conducted on all islets present on three sections (~ 50 µm interval) from each islet preparation using Image J software. Apoptosis was counted as the number of TUNEL and DAPI double-positive nuclei relative to total number of DAPI-positive nuclei. Amyloid deposition was computed as the islet area occupied by ThioS staining.

Transgenic rat studies

Hemizygous hIAPP transgenic male rats (RIP-HAT or CD:SD-Tg(ins2-IAPP)Soel) and wild-type male Sprague-Dawley rats were obtained from Charles River Laboratories (Germany) and housed under controlled conditions (21±1ºC, 12:12 hour light/dark cycle with light phase from 2:00 am to 2:00 pm) with free access to standard chow diet (Extrudate 3436, KLIBA NAFAG, Switzerland) and water. Rats were

randomized based on body weight and blood glucose concentration during oral glucose tolerance test and received a once-weekly intraperitoneal (i.p.) injection of recombinant rat chimeric antibody (^{ch}α-IAPP-O and ^{ch}α-IAPP-O/F) or PBS at a volumetric dose of 2 ml/kg. Rats were weighed every week to determine the dose of antibody injected. Metformin (1,1-Dimethylbiguanide hydrochloride, 97%; D150959, Sigma) was supplied in drinking water (3 to 3.8 g/L). Daily water intake was estimated by weighing the water bottles and metformin concentration was adjusted accordingly to reach a target dose of 200 mg/kg/day. Treatments started at 12 weeks of age and were blinded until full completion of the studies.

Oral glucose tolerance test (oGTT) was performed on fasted rats (12h overnight fasting with free access to water). Rats were orally administered with 2 g/kg glucose (50% solution, B. Braun Medical AG) and blood samples were repeatedly collected (0, 15, 30, 60, 120 and 240 min) from the sublingual vein under gas anaesthesia (3% isoflurane, Zoetis, Switzerland). Blood glucose and glycated hemoglobin (HbA1c) were measured using a Contour XT glucometer (Bayer) and A1CNow+ test kit (Bayer), respectively. Plasma was isolated by centrifugation and insulin levels were determined by ELISA (rat insulin ELISA, Mercodia). Beta cell function was estimated by $BCI_{oral} = AUC_{insulin}/AUC_{glucose}$ (AUC, area under the concentration curves during oGTT)[68].

Following a washout period of three weeks without any treatment (equivalent to the plasma half-life of rat ^{ch}α-IAPP-O), and three days prior to sacrifice, rats received a single intraperitoneal administration of human α-IAPP-O (30 mg/kg, i.p.) for histological measurement of α-IAPP-O-bound hIAPP aggregates in pancreatic islets (*in vivo* target engagement). Rats were euthanized by sodium pentobarbital injection (60 mg/kg i.p.) and pancreas tissue was removed, weighted, and cut in three parts corresponding to pancreas head, core and tail. A small piece of pancreas tail was dissected out, weighted, flash frozen in liquid nitrogen, homogenized (10%, w/v) in modified RIPA buffer (50 mM Tris-HCl pH 7.4, 150 mM NaCl, 1 mM EDTA, 5% NP-40, 0.5% Sodium deoxycholate, 0.1% SDS) and centrifuged (100’000 g, 4°C, 30 min). Supernatant was collected and pellet was solubilized by sonication in 70% formic acid. Supernatants and pellets were kept stored at -80°C until analyzed for soluble and insoluble IAPP content by ELISA (EZHA-52K, Millipore). The other parts of the pancreas were fixed in 4% paraformaldehyde (w/v) and embedded in paraffin, or frozen in OCT medium (following soaking in 30% sucrose) for histological analyses. Animal experiments were approved by Zürich cantonal authorities and performed as recommended by the Federal Veterinary Office (FVO).

Human islet transplant into NSG and Rag2$^{-/-}$ mice

NSG male mice (NOD.Cg-*Prkdc*^{scid} *Il2rg*^{tm1Wjl}/Sz, #005557, The Jackson Laboratory, USA) aged 6 to 20 weeks, and made diabetic by intraperitoneal injection of 180 mg/kg streptozotocin, were transplanted with 280-340 human islets under the kidney capsule. Human islets from non-diabetic, cadaveric donors (additional information is provided in **Supplementary Table 2**) were obtained from Prodo Laboratories (Aliso Viejo, USA) and the Alberta Diabetes Institute Islet Core (Edmonton, Canada), hand-picked to 99%

purity and cultured overnight with 10 µg/mL mouse ^{ch}α-IAPP-O or isotype control antibody in complete CMRL media (containing 100 U/mL penicillin, 100 µg/mL streptomycin, 0.05 mg/mL gentamicin, and 2 mmol/L glutamax) prior to transplantation.

Rag2 null male mice (B6.129S6-*Rag2*^{tm1Fwa} N12, #RAGN12-M, Taconic Biosciences, Lille Skensved, DK) aged 13 to 57 weeks were transplanted with 450 human islets isolated from non-diabetic brain-dead donors (obtained from the Centre Hospitalier Régional Universitaire de Lille, France; additional information in **Supplementary Table 2**) and placed on a high-fat diet (Brogaarden – Research Diets Inc., Denmark) two weeks post-transplant.

Mice were injected with 10 mg/kg mouse ^{ch}α-IAPP-O or isotype control antibody intraperitoneally (i.p.), starting one day prior transplant (NSG mice) and two- or eight-weeks post-transplant (Rag2 null mice), and subsequently once weekly for the duration of the studies. Oral glucose tolerance test (3 g/kg glucose) and blood glucose measurement were performed following a 5-hour fast. Plasma total insulin (mouse and human) and human C-peptide levels were determined by ELISA (mouse insulin and human C-peptide ELISA, Mercodia). Mice were injected with human α-IAPP-O (30 mg/kg, i.p.) three days before sacrifice to measure the amount of hIAPP aggregates in human islet grafts. Graft-bearing kidneys were frozen in OCT medium, and 5-µm sections were cut for histology. Studies were approved by the Animal Care Committee and the Clinical Research Ethics Board of the University of British Columbia, and by the institutional ethical committee of the University of Lille and the Centre Hospitalier Régional Universitaire de Lille.

Histology

Formalin fixed paraffin-embedded human (obtained from University Hospital Basel, Switzerland) and rat pancreas, and OCT-embedded fresh rat pancreas and human islet graft-bearing kidneys were cut in 5 µm-sections. Paraffin-embedded sections were deparaffinized, rehydrated, and immersed in antigen retrieval solution (70% formic acid) for 10 min. For DAB-based staining, endogenous peroxidase activity was quenched with 3% H_20_2 in methanol for 10 min. Fixed and frozen sections were blocked in PBS + 2.5% horse serum + 2.5% goat serum + 4% BSA for 1h, and incubated with mouse chimeric ^{ch}α-IAPP-O, mouse monoclonal anti-IAPP (1:100; R10/99, Abcam), mouse monoclonal anti-human IAPP (1:100; E-5, Santa Cruz Biotechnology), guinea pig polyclonal anti-insulin antibody (1:3; FLEX, Dako), mouse monoclonal anti-rat CD68 (1:1000; MCA341GA, Bio-Rad), and rat monoclonal anti-mouse CD68 antibody (1:200; ab53444, Abcam). Peroxidase-based staining was performed using biotinylated donkey anti-mouse secondary antibody (1:500; Jackson ImmunoResearch) combined with Vectastain ABC detection (Vector Laboratories). Fluorescence detection was achieved using Cy5- , Cy3- and Alexa 488-conjugated donkey anti-mouse (1:200), TRITC-conjugated goat anti-guinea pig (1:200), and Cy3-conjugated mouse anti-rat (1:200) secondary antibodies (Jackson ImmunoResearch). Amyloid deposits were stained using 0.15% (w/v) thioflavin-S (ThioS, Sigma) in H_2O followed by rinsing in ethanol 70% and H_2O. α-IAPP-O-bound

hIAPP aggregates (*in vivo* target engagement) were revealed on fresh frozen tissue sections using Cy5-conjugated donkey anti-human secondary antibody (1:200). Slides were mounted using Hydromount media (National Diagnostics). Bright-field imaging was performed on a Dotslide VS120 slide scanner (Olympus) and fluorescence imaging on a Leica SP8 confocal laser scanning microscope. Islet area, insulin- and hIAPP-immunoreactive beta cell content were analyzed on all islets (> 2500 μm^2) identified on paraffin-embedded rat pancreas head, core and tail (four sections each per rat). α-IAPP-O-bound hIAPP aggregates, ThioS-positive amyloid, and CD68-immunoreactive macrophages present within islets were quantified on rat pancreas and human islet graft cryosections (four and three to six sections per tissue, respectively). Data were computed as the fluorescence area above a predetermined threshold using Image-Pro Premier software (Media Cybernetics) and expressed as percentage of corresponding islet and tissue area. Colocalization between CD68-immunoreactive macrophages and α-IAPP-O-bound hIAPP aggregates or ThioS-positive amyloid was analyzed using ImageJ/FiJi software. Beta cell mass (mg) was calculated as follows: (Σ insulin-positive area / pancreas area) x pancreas weight (mg).

Phagocytosis assay

Peripheral blood mononuclear cells (PBMCs) were enriched from healthy donor blood using monocyte isolation kit (Miltenyi Biotec) and differentiated into macrophages in serum-free medium (M-SFM, ThermoFisher Scientific) supplemented with 100 ng/mL GM-CSF (Gibco) and 100 µg/ml penicillin/streptomycin for 6 days at 37°C and 5% CO_2. PBMC-derived macrophages were plated (5 x 10^5 cells/well) and cultured in M-SFM medium supplemented with 100 µg/ml penicillin/streptomycin, 100 ng/mL GM-CSF, 1 ng/mL LPS (Sigma) and 20 ng/mL IFN-γ one day prior to the experiment.

Lyophilized hIAPP peptide was reconstituted in 0.1 M sodium bicarbonate buffer (pH 8.4) to a final peptide concentration of 4 mg/ml, incubated with pHrodo green STP ester dye (20 mg/ml in DMSO; P35369, ThermoFisher Scientific) for 30 min at room temperature in the dark, lyophilized with an Alpha 1-2 LDplus freeze dryer (Christ) and stored at -20°C until use. Lyophilized pHrodo-labeled hIAPP and unlabeled hIAPP were reconstituted (1:3) in serum-free RPMI-1640 medium (Gibco) to a final concentration of 5 and 15 µM, respectively. Human α-IAPP-O, inert α-IAPP-O or IgG control antibody were added at various concentrations, followed by incubation for 2h at room temperature under quiescent conditions.

PBMC-derived macrophages were incubated with a 1:10 dilution of the solution containing pHrodo-labeled hIAPP aggregates (20 µM) and antibodies (0, 1.5, 3, 6 and 12 nM) in fresh M-SFM medium supplemented with 100 µg/ml penicillin/streptomycin and 50 µg/mL of the scavenger receptor inhibitor Fucoidan (F5631, Sigma) for 30min at 37°C. Human Fc receptor (FcR) blocking solution (1:10 dilution; 130-059-901, Miltenyi Biotec) and cytochalasin D (50 µg/ml; C2618, Sigma) were added to inhibit FcR-dependent and general phagocytosis. After detachment, macrophages were washed in PBS and fluorescence of any surface-bound pHrodo-labeled hIAPP was quenched by addition of trypan blue (10%),

and phagocytosis was analyzed using a FACS Aria II flow cytometer equipped with BD FACS Diva software (BD Biosciences). Intracellular pHrodo green was excited using a 488 nm laser and the fluorescence emission was collected using a 530/30 nm filter (FITC). A total of 10’000 events were acquired from each sample and data were exported as Flow Cytometry Standard format 3.0 files (FCS files) and analyzed with FlowJo software (Tree Star Inc.). Gating was done on single macrophages with high forward and side scatter (FSC-A and SSC-A) levels, and pHrodo-hIAPP-positive macrophages with fluorescence emission above cytochalasin D-treated macrophages (negative control) were counted.

Statistical analysis

Data are expressed as means ± s.e.m and results between groups were analyzed using Student’s t-test, one-way and two-way ANOVA with post hoc tests for multiple comparisons. Statistical analyses were conducted using GraphPad PRISM 7 (GraphPad Software, USA) and significance was set at *$p<0.05$, **$p<0.01$, ***$p<0.001$ and ****$p<0.0001$.

Declarations

Author contributions

F.D.H and F.W. designed the experiments and analyzed the data. F.D.H prepared the manuscript. C.S., I.C. and K.B. performed experiments. H.C.D. and J.T. conducted the human islet graft experiments. H.C.D., M.O., P.A., J.K-C., C.B.V., T.L. contributed to the experimental design and interpretation of the results. M.D. provided human tissues and critically reviewed the manuscript. C.H., R.N. and J.G. supervised the project. All authors approved the final version of the manuscript.

Acknowledgements

We are grateful to Winnie Gut, Kerstin Linder, Leoni Hugentobler, Erika Tarasco, Ines Rito Brandao, Alexandra Durrer, Maik Krüger, Marie Kopp, Fulvio Grigolato, Anna Jeske, Daniel Schuppli, Petra Borter, Luzia Senn and Nadine Glassl for technical help, Benoît Combaluzier for help on antibody discovery and production processes, Fabian Buller for reviewing the manuscript and Tobias Welt for conceptual contribution. We acknowledge staff members of the Center for Microscopy and Image Analysis of the University of Zürich (ZMB). This work was supported by CTI grants 13750.1 PFFLE-LS and 17448.1 PFLS-LS to M.D., T.L. and R.N, by Canadian Institutes of Health Research grants PJT-165943 and PJT-156449 to C.B.V, and by JDRF postdoctoral fellowships 3-PDF-2014-191-A-N and 3-APF-2018-586-A-N to H.C.D. The authors declare no conflict of interest.

Declaration of interests

F.D.H., F.W., C.S., I.C., K.B., C.H., R.N. and J.G. are employees and shareholders of Neurimmune; J.G., F.D.H., F.W., and I.C. are inventors on patents related to this work.

References

1. Mukherjee, A., Morales-Scheihing, D., Butler, P. C. & Soto, C. Type 2 diabetes as a protein misfolding disease. *Trends Mol Med* **21**, 439–449 (2015).
2. Westermark, P., Andersson, A. & Westermark, G. T. Islet amyloid polypeptide, islet amyloid, and diabetes mellitus. *Physiol. Rev.* **91**, 795–826 (2011).
3. Lutz, T. A. Control of energy homeostasis by amylin. *Cell. Mol. Life Sci.* **69**, 1947–1965 (2012).
4. Jurgens, C. A. *et al.* β-cell loss and β-cell apoptosis in human type 2 diabetes are related to islet amyloid deposition. *Am. J. Pathol.* **178**, 2632–2640 (2011).
5. Abedini, A. & Schmidt, A. M. Mechanisms of islet amyloidosis toxicity in type 2 diabetes. *FEBS Lett.* **587**, 1119–1127 (2013).
6. Raleigh, D., Zhang, X., Hastoy, B. & Clark, A. The β-cell assassin: IAPP cytotoxicity. *J. Mol. Endocrinol.* **59**, R121–R140 (2017).
7. Sakagashira, S. *et al.* S20G mutant amylin exhibits increased in vitro amyloidogenicity and increased intracellular cytotoxicity compared to wild-type amylin. *Am. J. Pathol.* **157**, 2101–2109 (2000).
8. Ma, Z. *et al.* Enhanced in vitro production of amyloid-like fibrils from mutant (S20G) islet amyloid polypeptide. *Amyloid* **8**, 242–249 (2001).
9. Novials, A., Rojas, I., Casamitjana, R., Usac, E. F. & Gomis, R. A novel mutation in islet amyloid polypeptide (IAPP) gene promoter is associated with Type II diabetes mellitus. *Diabetologia* **44**, 1064–1065 (2001).
10. Ma, Z., Westermark, G. T., Johnson, K. H., O'Brien, T. D. & Westermark, P. Quantitative immunohistochemical analysis of islet amyloid polypeptide (IAPP) in normal, impaired glucose tolerant, and diabetic cats. *Amyloid* **5**, 255–261 (1998).
11. Guardado Mendoza, R. *et al.* Delta cell death in the islet of Langerhans and the progression from normal glucose tolerance to type 2 diabetes in non-human primates (baboon, Papio hamadryas). *Diabetologia* **58**, 1814–1826 (2015).
12. Guardado-Mendoza, R. *et al.* Pancreatic islet amyloidosis, beta-cell apoptosis, and alpha-cell proliferation are determinants of islet remodeling in type-2 diabetic baboons. *Proc. Natl. Acad. Sci. U.S.A.* **106**, 13992–13997 (2009).
13. Hull, R. L. *et al.* Increased dietary fat promotes islet amyloid formation and beta-cell secretory dysfunction in a transgenic mouse model of islet amyloid. *Diabetes* **52**, 372–379 (2003).
14. Höppener, J. W. M. *et al.* Human islet amyloid polypeptide transgenic mice: in vivo and ex vivo models for the role of hIAPP in type 2 diabetes mellitus. *Exp Diabetes Res* **2008**, 697035 (2008).

15. Butler, A. E. *et al.* Diabetes due to a progressive defect in beta-cell mass in rats transgenic for human islet amyloid polypeptide (HIP Rat): a new model for type 2 diabetes. *Diabetes* **53**, 1509–1516 (2004).
16. Matveyenko, A. V. & Butler, P. C. Beta-cell deficit due to increased apoptosis in the human islet amyloid polypeptide transgenic (HIP) rat recapitulates the metabolic defects present in type 2 diabetes. *Diabetes* **55**, 2106–2114 (2006).
17. Zou, X. *et al.* Preparation of a new type 2 diabetic miniature pig model via the CRISPR/Cas9 system. *Cell Death Dis* **10**, (2019).
18. Potter, K. J. *et al.* Amyloid inhibitors enhance survival of cultured human islets. *Biochim. Biophys. Acta* **1790**, 566–574 (2009).
19. Andersson, A. *et al.* Amyloid deposition in transplanted human pancreatic islets: a conceivable cause of their long-term failure. *Exp Diabetes Res* **2008**, 562985 (2008).
20. Bohman, S. & Westermark, G. T. Extensive amyloid formation in transplanted microencapsulated mouse and human islets. *Amyloid* **19**, 87–93 (2012).
21. Abedini, A. *et al.* Time-resolved studies define the nature of toxic IAPP intermediates, providing insight for anti-amyloidosis therapeutics. *Elife* **5**, (2016).
22. Last, N. B., Rhoades, E. & Miranker, A. D. Islet amyloid polypeptide demonstrates a persistent capacity to disrupt membrane integrity. *Proc. Natl. Acad. Sci. U.S.A.* **108**, 9460–9465 (2011).
23. Caillon, L., Hoffmann, A. R. F., Botz, A. & Khemtemourian, L. Molecular Structure, Membrane Interactions, and Toxicity of the Islet Amyloid Polypeptide in Type 2 Diabetes Mellitus. *J Diabetes Res* **2016**, 5639875 (2016).
24. Huang, C. *et al.* High expression rates of human islet amyloid polypeptide induce endoplasmic reticulum stress mediated beta-cell apoptosis, a characteristic of humans with type 2 but not type 1 diabetes. *Diabetes* **56**, 2016–2027 (2007).
25. Matveyenko, A. V., Gurlo, T., Daval, M., Butler, A. E. & Butler, P. C. Successful versus failed adaptation to high-fat diet-induced insulin resistance: the role of IAPP-induced beta-cell endoplasmic reticulum stress. *Diabetes* **58**, 906–916 (2009).
26. Westwell-Roper, C. Y., Ehses, J. A. & Verchere, C. B. Resident macrophages mediate islet amyloid polypeptide-induced islet IL-1β production and β-cell dysfunction. *Diabetes* **63**, 1698–1711 (2014).
27. Masters, S. L. *et al.* Activation of the NLRP3 inflammasome by islet amyloid polypeptide provides a mechanism for enhanced IL-1β in type 2 diabetes. *Nat. Immunol.* **11**, 897–904 (2010).
28. Cohen, S. I. A. *et al.* A molecular chaperone breaks the catalytic cycle that generates toxic Aβ oligomers. *Nat. Struct. Mol. Biol.* **22**, 207–213 (2015).
29. Arosio, P. *et al.* Kinetic analysis reveals the diversity of microscopic mechanisms through which molecular chaperones suppress amyloid formation. *Nat Commun* **7**, 10948 (2016).
30. Habchi, J. *et al.* Systematic development of small molecules to inhibit specific microscopic steps of Aβ42 aggregation in Alzheimer's disease. *Proc. Natl. Acad. Sci. U.S.A.* **114**, E200–E208 (2017).

31. Munke, A. *et al.* Phage display and kinetic selection of antibodies that specifically inhibit amyloid self-replication. *Proc. Natl. Acad. Sci. U.S.A.* **114**, 6444–6449 (2017).
32. Arosio, P., Vendruscolo, M., Dobson, C. M. & Knowles, T. P. J. Chemical kinetics for drug discovery to combat protein aggregation diseases. *Trends Pharmacol. Sci.* **35**, 127–135 (2014).
33. Lorenzo, A. & Yankner, B. A. Beta-amyloid neurotoxicity requires fibril formation and is inhibited by congo red. *Proc. Natl. Acad. Sci. U.S.A.* **91**, 12243–12247 (1994).
34. Matveyenko, A. V. *et al.* Beneficial endocrine but adverse exocrine effects of sitagliptin in the human islet amyloid polypeptide transgenic rat model of type 2 diabetes: interactions with metformin. *Diabetes* **58**, 1604–1615 (2009).
35. Hunter, R. W. *et al.* Metformin reduces liver glucose production by inhibition of fructose-1-6-bisphosphatase. *Nat. Med.* **24**, 1395–1406 (2018).
36. Westwell-Roper, C., Denroche, H. C., Ehses, J. A. & Verchere, C. B. Differential Activation of Innate Immune Pathways by Distinct Islet Amyloid Polypeptide (IAPP) Aggregates. *J. Biol. Chem.* **291**, 8908–8917 (2016).
37. Andersson, A. *et al.* Amyloid deposition in transplanted human pancreatic islets: a conceivable cause of their long-term failure. *Exp Diabetes Res* **2008**, 562985 (2008).
38. Potter, K. J. *et al.* Islet amyloid deposition limits the viability of human islet grafts but not porcine islet grafts. *Proc. Natl. Acad. Sci. U.S.A.* **107**, 4305–4310 (2010).
39. Bohman, S. & Westermark, G. T. Extensive amyloid formation in transplanted microencapsulated mouse and human islets. *Amyloid* **19**, 87–93 (2012).
40. Gargani, S. *et al.* Adaptive changes of human islets to an obesogenic environment in the mouse. *Diabetologia* **56**, 350–358 (2013).
41. Davies, M. J. *et al.* Management of hyperglycaemia in type 2 diabetes, 2018. A consensus report by the American Diabetes Association (ADA) and the European Association for the Study of Diabetes (EASD). *Diabetologia* **61**, 2461–2498 (2018).
42. Engel, M. F. M. Membrane permeabilization by Islet Amyloid Polypeptide. *Chem. Phys. Lipids* **160**, 1–10 (2009).
43. Christensen, M., Skeby, K. K. & Schiøtt, B. Identification of Key Interactions in the Initial Self-Assembly of Amylin in a Membrane Environment. *Biochemistry* **56**, 4884–4894 (2017).
44. Zraika, S. *et al.* Oxidative stress is induced by islet amyloid formation and time-dependently mediates amyloid-induced beta cell apoptosis. *Diabetologia* **52**, 626–635 (2009).
45. Park, Y. J. *et al.* The role of caspase-8 in amyloid-induced beta cell death in human and mouse islets. *Diabetologia* **57**, 765–775 (2014).
46. Ritzel, R. A., Meier, J. J., Lin, C.-Y., Veldhuis, J. D. & Butler, P. C. Human islet amyloid polypeptide oligomers disrupt cell coupling, induce apoptosis, and impair insulin secretion in isolated human islets. *Diabetes* **56**, 65–71 (2007).

47. Rivera, J. F., Costes, S., Gurlo, T., Glabe, C. G. & Butler, P. C. Autophagy defends pancreatic β cells from human islet amyloid polypeptide-induced toxicity. *J. Clin. Invest.* **124**, 3489–3500 (2014).
48. Abedini, A., Derk, J. & Schmidt, A. M. The receptor for advanced glycation endproducts is a mediator of toxicity by IAPP and other proteotoxic aggregates: Establishing and exploiting common ground for novel amyloidosis therapies. *Protein Sci.* **27**, 1166–1180 (2018).
49. Badman, M. K., Pryce, R. A., Chargé, S. B., Morris, J. F. & Clark, A. Fibrillar islet amyloid polypeptide (amylin) is internalised by macrophages but resists proteolytic degradation. *Cell Tissue Res.* **291**, 285–294 (1998).
50. Van Hulle, F. *et al.* Formation of amyloid in encapsulated human pancreatic and human stem cell-generated beta cell implants. *Am J Transplant* (2020) doi:10.1111/ajt.16398.
51. Fonseca, V. A. Defining and Characterizing the Progression of Type 2 Diabetes. *Diabetes Care* **32**, S151–S156 (2009).
52. Salunkhe, V. A., Veluthakal, R., Kahn, S. E. & Thurmond, D. C. Novel approaches to restore beta cell function in prediabetes and type 2 diabetes. *Diabetologia* **61**, 1895–1901 (2018).
53. Gurzov, E. N., Ke, P. C., Ahlgren, U., Garcia Ribeiro, R. S. & Gotthardt, M. Novel Strategies to Protect and Visualize Pancreatic β Cells in Diabetes. *Trends Endocrinol Metab* **31**, 905–917 (2020).
54. Aston-Mourney, K. *et al.* One year of sitagliptin treatment protects against islet amyloid-associated β-cell loss and does not induce pancreatitis or pancreatic neoplasia in mice. *Am J Physiol Endocrinol Metab* **305**, E475–E484 (2013).
55. Jurczyk, A. *et al.* Improved function and proliferation of adult human beta cells engrafted in diabetic immunodeficient NOD-scid IL2rγnull mice treated with alogliptin. *Diabetes Metab Syndr Obes* **6**, 493–499 (2013).
56. Yang, C. *et al.* Lixisenatide accelerates restoration of normoglycemia and improves human beta-cell function and survival in diabetic immunodeficient NOD-scid IL-2rg(null) RIP-DTR mice engrafted with human islets. *Diabetes Metab Syndr Obes* **8**, 387–398 (2015).
57. Abdulreda, M. H., Rodriguez-Diaz, R., Caicedo, A. & Berggren, P.-O. Liraglutide Compromises Pancreatic β Cell Function in a Humanized Mouse Model. *Cell Metabolism* **23**, 541–546 (2016).
58. RISE Consortium. Lack of Durable Improvements in β-Cell Function Following Withdrawal of Pharmacological Interventions in Adults With Impaired Glucose Tolerance or Recently Diagnosed Type 2 Diabetes. *Diabetes Care* **42**, 1742–1751 (2019).
59. RISE Consortium & RISE Consortium Investigators. Effects of Treatment of Impaired Glucose Tolerance or Recently Diagnosed Type 2 Diabetes With Metformin Alone or in Combination With Insulin Glargine on β-Cell Function: Comparison of Responses In Youth And Adults. *Diabetes* **68**, 1670–1680 (2019).
60. van Raalte, D. H. & Verchere, C. B. Improving glycaemic control in type 2 diabetes: Stimulate insulin secretion or provide beta-cell rest? *Diabetes Obes Metab* **19**, 1205–1213 (2017).
61. Sevigny, J. *et al.* The antibody aducanumab reduces Aβ plaques in Alzheimer's disease. *Nature* **537**, 50–56 (2016).

62. Weihofen, A. *et al.* Development of an aggregate-selective, human-derived α-synuclein antibody BIIB054 that ameliorates disease phenotypes in Parkinson's disease models. *Neurobiol. Dis.* **124**, 276–288 (2019).
63. Maier, M. *et al.* A human-derived antibody targets misfolded SOD1 and ameliorates motor symptoms in mouse models of amyotrophic lateral sclerosis. *Sci Transl Med* **10**, (2018).
64. Nguyen, L. *et al.* Antibody Therapy Targeting RAN Proteins Rescues C9 ALS/FTD Phenotypes in C9orf72 Mouse Model. *Neuron* (2019) doi:10.1016/j.neuron.2019.11.007.
65. Meisl, G. *et al.* Molecular mechanisms of protein aggregation from global fitting of kinetic models. *Nat Protoc* **11**, 252–272 (2016).
66. Kerr-Conte, J. *et al.* Upgrading pretransplant human islet culture technology requires human serum combined with media renewal. *Transplantation* **89**, 1154–1160 (2010).
67. Henquin, J.-C., Dufrane, D., Kerr-Conte, J. & Nenquin, M. Dynamics of glucose-induced insulin secretion in normal human islets. *Am. J. Physiol. Endocrinol. Metab.* **309**, E640-650 (2015).
68. Pacini, G., Omar, B. & Ahrén, B. Methods and models for metabolic assessment in mice. *J Diabetes Res* **2013**, 986906 (2013).

Figures

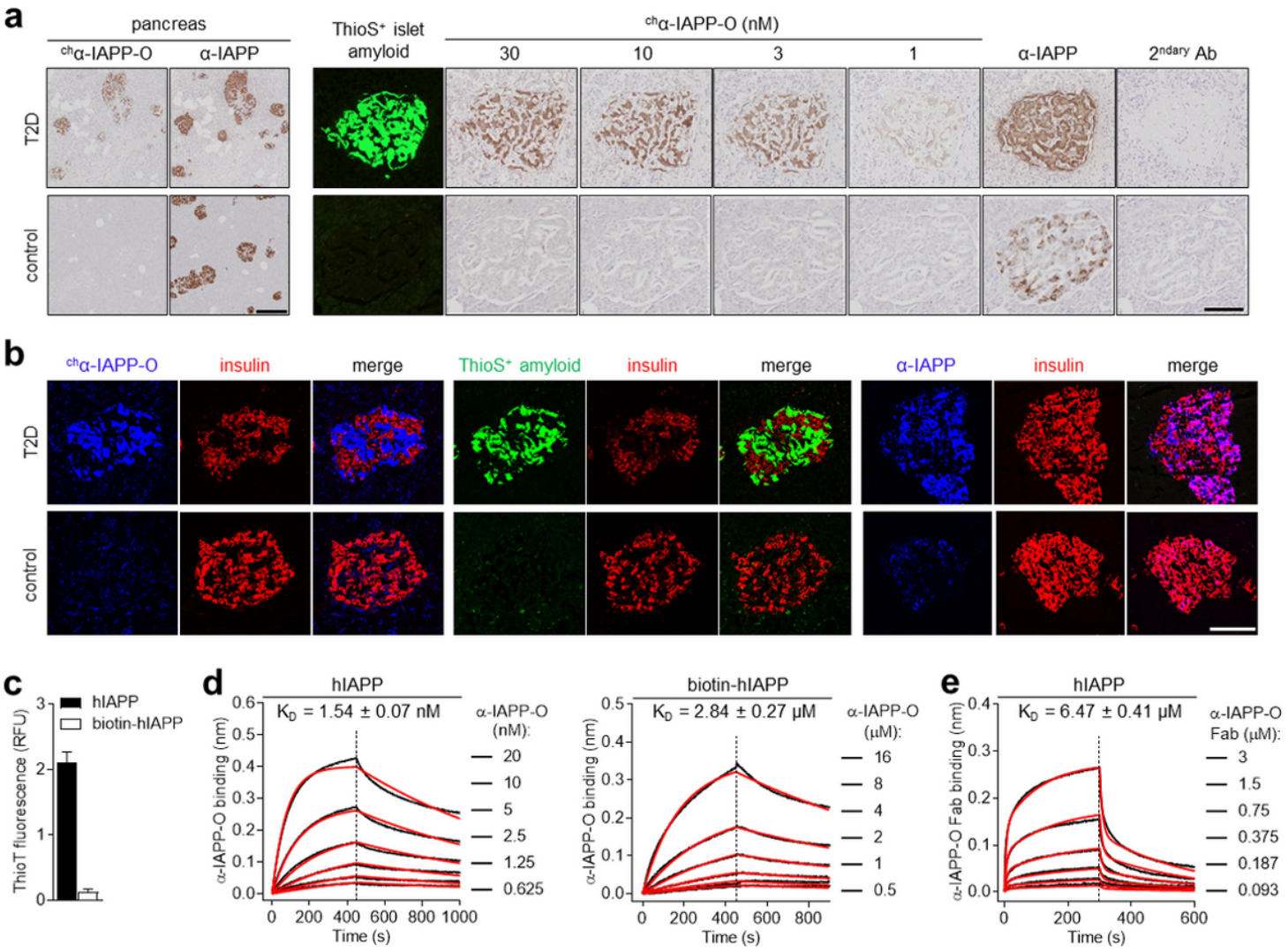

Figure 1

α-IAPP-O antibody selectively binds to disease-relevant extracellular IAPP aggregates. (a) Representative images of pancreas (left panel) and individual pancreatic islets (right panel) from a human type-2 diabetes (T2D) and a non-diabetic control subject stained with mouse chimeric α-IAPP-O (chα-IAPP-O, 30 nM or at indicated concentrations) and with a mouse anti-IAPP antibody that binds aggregated and monomeric IAPP species (α-IAPP) on adjacent sections. Islet amyloid fibrils were stained with thioflavin-S (ThioS) and anti-mouse secondary antibody was used as control (2ndary Ab). Scale bars: 300 and 100 μm, respectively. (b) Representative images of T2D and control human pancreatic islets stained with mouse chimeric α-IAPP-O (chα-IAPP-O, 30 nM; in blue, left panel), ThioS for extracellular amyloid deposits (in green, middle panel) and α-IAPP for physiological human IAPP (in blue, right panel). Beta cells were visualized using anti-insulin antibody (in red) and merged images are shown. Scale bar: 100 μm. (c) Aggregation propensity of human IAPP (hIAPP) and biotinylated human IAPP (biotin-hIAPP) in solution measured by thioflavin-T (ThioT) fluorescence. Data are means ± s.e.m. from four replicates. (d) Binding kinetic analysis of α-IAPP-O to hIAPP (left panel) and biotin-hIAPP (right panel) using biolayer interferometry (BLI). (e) BLI analysis of α-IAPP-O Fab binding to hIAPP. BLI dose-response association

and dissociation curves (black line), fitting curves (red line) and KD constants (means ± s.e.m.) are derived from three independent runs (detailed in Supplementary Table 1). Association and dissociation are separated by a dashed line.

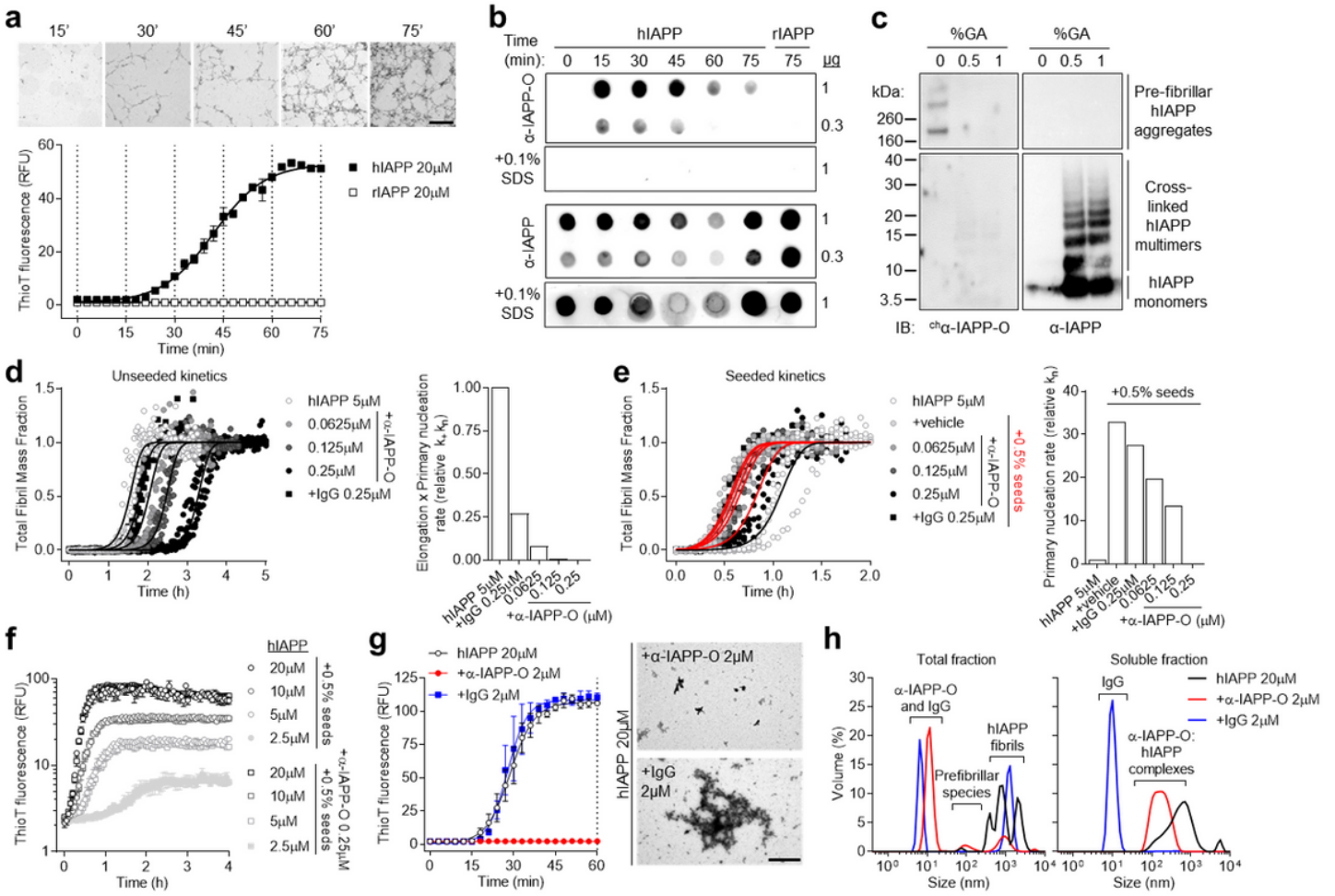

Figure 2

α-IAPP-O interacts with transient pre-fibrillar hIAPP oligomers. (a) Time course of amyloid fibril formation of hIAPP and rodent IAPP (rIAPP) in solution monitored by transmission electron microscopy (TEM; top inset; magnification: 1.05 k; scale bar: 10 μm) and ThioT fluorescence (bottom). Data are means ± s.e.m. of five (hIAPP) and three (rIAPP) replicates. Dotted lines indicate time points of sampling for TEM and immunoblotting. (b) Dot blot analysis of fractions collected over the course of amyloid formation and detected with α-IAPP-O and a non-selective α-IAPP antibody. Spotted fractions contained 1 and 0.3 μg of IAPP and 0.1% SDS was added to denature aggregates. (c) Immunoblotting of prefibrillar hIAPP aggregates and hIAPP monomers cross-linked with 0.5 and 1% glutaraldehyde (GA) using chα-IAPP-O and α-IAPP antibodies. (d) hIAPP aggregation kinetics in the presence of α-IAPP-O and IgG control antibody (left panel). Solid lines represent fitting to experimental data and the resulting product of elongation and primary nucleation (k+kn, right panel) using a model describing secondary nucleation-dominated aggregation. (e) Influence of α-IAPP-O on the aggregation kinetics of hIAPP seeded with 0.5% monomer equivalent preformed fibrils (red lines, left panel) and on the primary nucleation rate (kn, right

panel). Detailed kinetic modelling is shown in Supplementary Figure 3, 4 and 5. (f) ThioT-monitored amyloid fibril formation as a function of initial hIAPP concentration supplemented with 0.5% seeds and 0.5% seeds pre-incubated with α-IAPP-O (0.25 μM). Data are means ± s.e.m. from triplicates. (g) Aggregation kinetics of hIAPP (20 μM) in the presence of α-IAPP-O and IgG control antibodies (2 μM) measured by thioflavin-T fluorescence (left panel). Data are means ± s.e.m of triplicates. Representative TEM images of hIAPP aggregates formed in presence of α-IAPP-O and IgG control (right panel) after 60 min of incubation (dotted line on left panel). Scale bar: 2 μm. (h) Size distribution in total and soluble fractions from the samples described in g (at 60 min) measured by dynamic light scattering (see also Supplementary Figure 6). Data represent the average of three measurements on two experimental replicates.

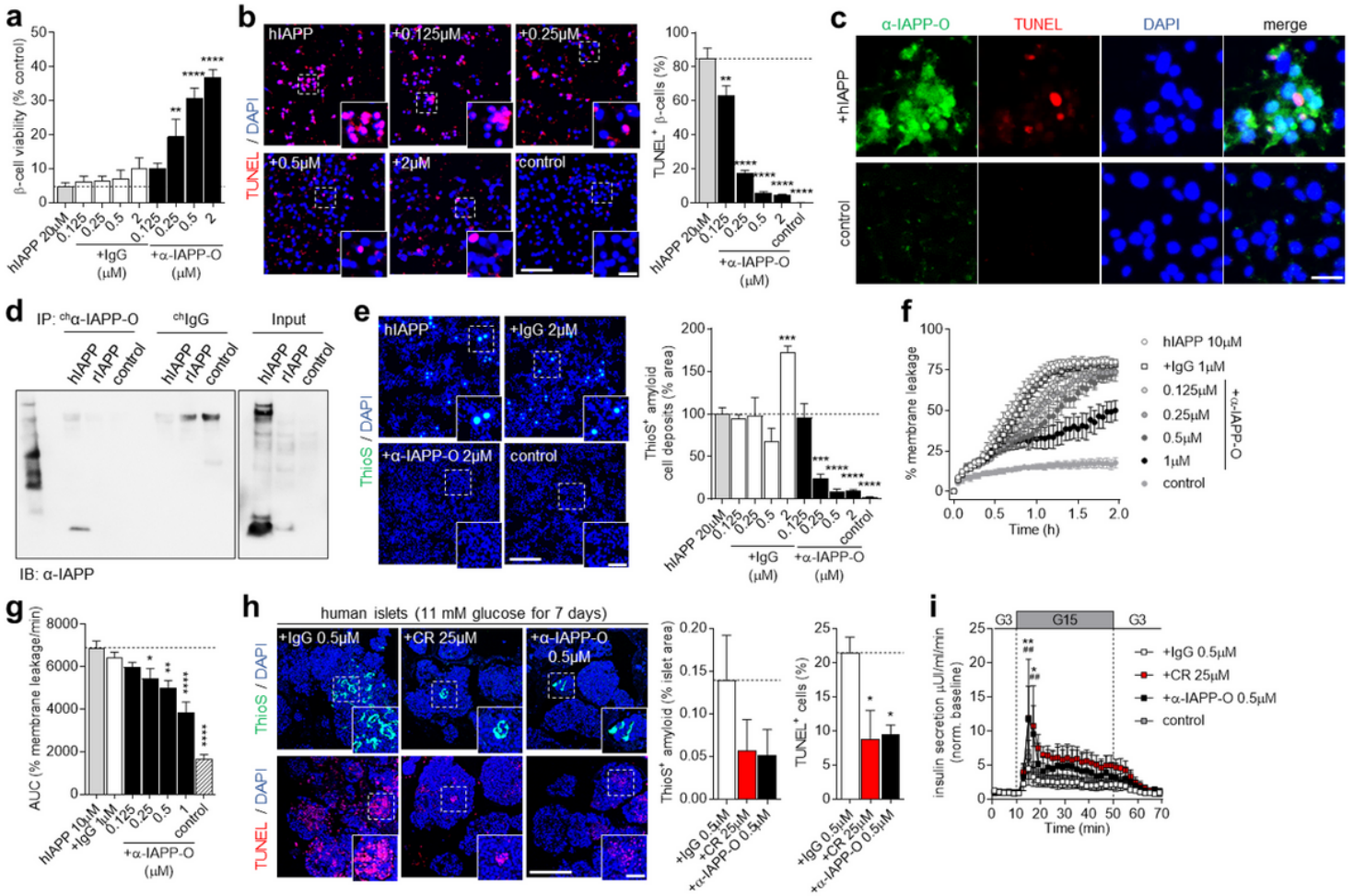

Figure 3

α-IAPP-O protects beta cells from toxicity induced by cell membrane-permeant hIAPP oligomers. (a) Viability of INS-1 beta cells exposed to hIAPP oligomers (hIAPP 20 μM) supplemented with α-IAPP-O (+α-IAPP-O) and IgG control (+IgG) at indicated concentrations (one-way ANOVA: $F(8,45)=19.52$, $P<0.0001$; post hoc Dunnett's multiple comparisons test +α-IAPP-O 0.25 μM versus hIAPP 20 μM: **P=0.0023, +α-IAPP-O 0.5 and 2 μM versus hIAPP 20 μM: ****P<0.0001). Data are from two independent experiments performed with three biological replicates. (b) Representative fluorescence microscopy images (left

panel) and quantification (right panel) of INS-1 beta cell apoptosis induced by hIAPP oligomers and visualized by TUNEL staining (in red) on DAPI-positive nuclei (in blue). Cells not exposed to hIAPP oligomers are used as control. Scale bars: 100 and 25 μm. Data are from three independent experiments (except +α-IAPP-O 0.125 μM and 0.25 μM concentrations from one and two experiments, respectively) performed with three biological replicates (one-way ANOVA: $F(5,39)=124.8$, $P<0.0001$; post hoc Dunnett's multiple comparisons test +α-IAPP-O 0.125 μM versus hIAPP 20 μM: **P=0.0031, +α-IAPP-O (0.25, 0.5 and 2 μM) and control versus hIAPP 20 μM: ****P<0.0001). (c) Representative images of immunofluorescence staining for hIAPP oligomers using α-IAPP-O (in green), TUNEL-positive apoptotic cells (in red) and INS-1 cell nuclei stained with DAPI (in blue). Scale bar: 25 μm. (d) Immunoprecipitation (IP) on cell membrane extracts of INS-1 cells exposed to hIAPP oligomers, rodent IAPP (rIAPP), and unexposed (control). Immunoblotting (IB) was performed using α-IAPP antibody. (e) Representative fluorescence microscopy images (left panel) and quantification (right panel) of ThioS-positive amyloid (in green) on INS-1 cells exposed to hIAPP oligomers (hIAPP 20 μM) supplemented with α-IAPP-O (+α-IAPP-O) and IgG control (+IgG) at indicated concentrations. Cell nuclei are visualized by DAPI (in blue). Scale bars: 300 and 100 μm. Data are from three biological replicates (one-way ANOVA: $F(9,20)=26.53$, $P<0.0001$; post hoc Dunnett's multiple comparisons test +α-IAPP-O 0.25 μM versus hIAPP 20 μM: ***P=0.0006, +α-IAPP-O (0.5 and 2 μM) and control versus hIAPP 20 μM: ****P<0.0001, +IgG 2 μM versus hIAPP 20 μM: ***P=0.0008). (f,g) Membrane leakage induced by hIAPP oligomers (hIAPP 10 μM) in the presence of α-IAPP-O (+α-IAPP-O) and IgG control (+IgG) at indicated concentrations and measured by time-lapse (f) and total fluorescence release (area under the curve, AUC) (g) from calcein-containing liposomes (one-way ANOVA: $F(6,42)=26.44$, $P<0.0001$; post hoc Dunnett's multiple comparisons test +α-IAPP-O 0.25 and 0.5 μM versus hIAPP 10 μM: *P=0.0266 and **P=0.0021, +α-IAPP-O 1 μM and control versus hIAPP 10 μM: ****P<0.0001). Data are from seven biological replicates from four independent experiments. (h) Human pancreatic islet immunofluorescence analysis upon culture in high glucose (11 mM) for seven days in the presence of α-IAPP-O (+α-IAPP-O 0.5 μM), IgG control (+IgG 0.5 μM) and Congo red (+CR 25 μM). Representative fluorescent images (left) and quantification (right) of ThioS-positive amyloid deposition (in green; one-way ANOVA: $F(2,6)=1.456$, $P=0.3052$; post hoc Dunnett's multiple comparisons test +α-IAPP-O 0.5 μM and +CR 25 μM versus +IgG 0.5 μM: P=0.2904 and P=0.3256) and apoptosis (in red; one-way ANOVA: $F(2,6)=6.047$, $P=0.0365$; post hoc Dunnett's multiple comparisons test +α-IAPP-O 0.5 μM and +CR 25 μM versus +IgG 0.5 μM: *P=0.0462 and *P=0.0374). DAPI-positive nuclei are stained in blue. Scale bars: 200 and 50 μm. (i) Insulin secretion from human islets cultured as shown in (h). Insulin response was measured at 3 (G3) and 15 mM (G15) glucose using dynamic perifusion (repeated measures two-way ANOVA (time x treatment): $F(102,272)=0.7278$, $P=0.9685$; post hoc Dunnett's multiple comparisons test +α-IAPP-O 0.5 μM versus +IgG 0.5 μM at 15 and 17 min: **P=0.0051 and *P=0.0182, +CR 25 μM versus +IgG 0.5 μM at 15 and 17 min: ##P=0.0040 and ##P=0.0037). Islets cultured in 5.5 mM glucose for seven days are used as control. Islet insulin content was comparable between conditions (see Supplementary Figure 7e). Data in (h,i) are from three independent experiments, each of them using islets from a different donor (detailed in Supplementary Table 2). All data are expressed as means ± s.e.m.

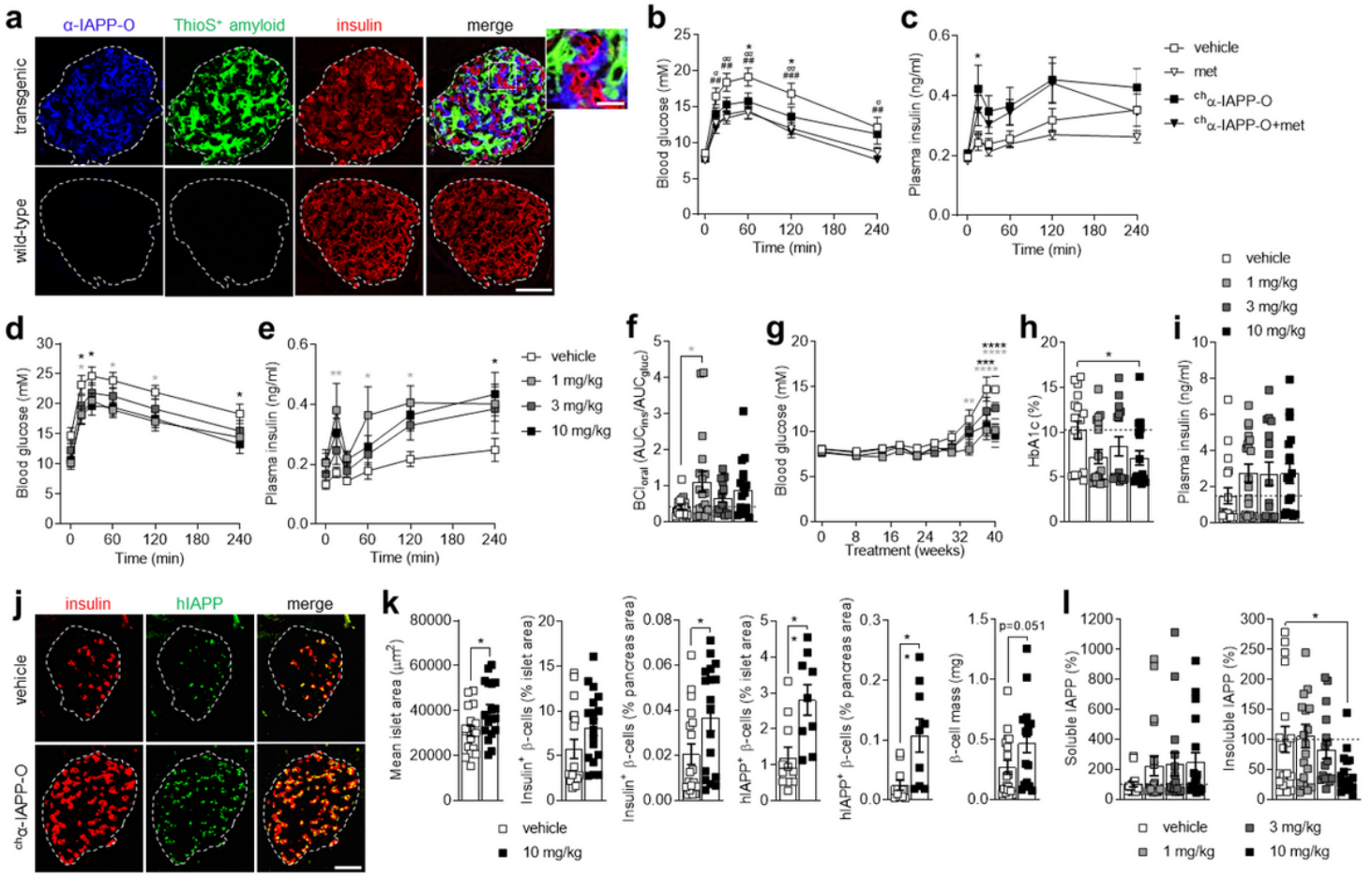

Figure 4

α-IAPP-O prevents diabetes progression and beta cell loss in hIAPP transgenic rats. (a) Representative immunofluorescence images of individual pancreatic islets from 57-week-old transgenic and wild-type rats stained for α-IAPP-O target engagement (in blue) three day after intraperitoneal administration (30 mg/kg). ThioS-positive islet amyloid fibrils (in green) and insulin-positive beta cells (in red) are shown. Scale bars: 100 and 25 µm. (b,c) Blood glucose concentration (b) and plasma insulin response (c) during an oral glucose tolerance test (oGTT) in 36-week-old hIAPP transgenic rats weekly injected (i.p.) with vehicle and rat chimeric α-IAPP-O (chα-IAPP-O, 3 mg/kg) for 24 weeks. Metformin (met; 200 mg/kg/day) served as an active comparator and was combined with chα-IAPP-O (chα-IAPP-O+met). Glucose tolerance improved in transgenic rats receiving chα-IAPP-O, met and chα-IAPP-O+met (repeated measures two-way ANOVA (time x treatment): $F(15,265)=2.466$, $P=0.0021$; post hoc Dunnett's multiple comparisons test chα-IAPP-O versus vehicle at 60 and 120 min: *P=0.0319 and *P=0.0486, met versus vehicle at 15, 30, 60, 120 and 240 min: σP=0.0232, σσP=0.0011, σσP=0.0012, σσP=0.0018 and σP=0.0393, and chα-IAPP-O+met versus vehicle at 15, 30, 60, 120 and 240 min: ##P=0.0070, ##P=0.0054, ##P=0.0032, ###P=0.0006 and ##P=0.0052). First phase insulin response to oGTT was increased in rats receiving chα-IAPP-O, and appeared to be increased in rats receiving chα-IAPP-O+met although not reaching statistical significance (repeated measures two-way ANOVA (time x treatment): $F(15,265)=1.629$, $P=0.0660$; post hoc Dunnett's multiple comparisons test chα-IAPP-O versus vehicle at 15 min: *P=0.0123, chα-IAPP-O+met versus

vehicle at 15 min: P=0.2449). Wild-type animals misgenotyped as transgenic were excluded from the study groups (n=2 vehicle, n=1 met, n=1 chα-IAPP-O+met). One animal died in the chα-IAPP-O+met group. Final group numbers were n=14 vehicle, n=14 met, n=16 chα-IAPP-O, n=13 chα-IAPP-O+met. (d,e) Blood glucose (d) and plasma insulin (e) levels during oGTT in 50-week-old transgenic rats administered with chα-IAPP-O at 1, 3 and 10 mg/kg i.p. for 38 weeks compared to vehicle treatment (n=18). (f) Beta cell function was estimated by BCIoral=AUCins/AUCgluc. (g) Development of hyperglycaemia in rats described in d-f. (h) HbA1c and (i) non-fasting plasma insulin after 41 weeks of treatment in transgenic rats described in d-g. chα-IAPP-O (1 and 10 mg/kg) treatment reduced blood glucose (repeated measures two-way ANOVA (time x treatment): F(15,335)=0.3657, P=0.9864; post hoc Dunnett's multiple comparisons test 1 mg/kg versus vehicle at 15, 60 and 120 min: *P=0.0397, *P=0.0428 and *P=0.0429, 10 mg/kg versus vehicle at 15, 30 and 240 min: *P=0.0379, *P=0.0413 and *P=0.0390) and increased plasma insulin levels during oGTT (repeated measures two-way ANOVA (time x treatment): F(15,335)=1.100, P=0.3553; post hoc Dunnett's multiple comparisons test 1 mg/kg versus vehicle at 15, 60 and 120 min: **P=0.0071, *P=0.0191 and *P=0.0175, 10 mg/kg versus vehicle at 240 min: *P=0.0212) due to improved beta cell function (one-way ANOVA: F(3,67)=2.612, P=0.0584; post hoc Dunnett's multiple comparisons test 1 mg/kg versus vehicle: *P=0.0256, 10 mg/kg versus vehicle: P=0.1846). chα-IAPP-O (1 and 10 mg/kg) also decreased fasting blood glucose (repeated measures two-way ANOVA (time x treatment): F(27,603)=1.787, P=0.0090; post hoc Dunnett's multiple comparisons test 1 mg/kg versus vehicle at 34, 38 and 40 weeks: **P=0.0034, ****P<0.0001 and ****P<0.0001, 10 mg/kg versus vehicle at 38 and 40 weeks: ***P=0.0003 and ****P<0.0001) and HbA1c (one-way ANOVA: F(3,67)=2.621, P=0.0578; post hoc Dunnett's multiple comparisons test 1 mg/kg versus vehicle: P=0.0520, 10 mg/kg versus vehicle: *P=0.0432), and seemed to enhance non-fasting plasma insulin levels without reaching statistical significance (one-way ANOVA: F(3,67)=1.395, P=0.2519; post hoc Dunnett's multiple comparisons test 1 mg/kg versus vehicle: P=0.2139, 10 mg/kg versus vehicle: P=0.2356). The 3 mg/kg dose failed to significantly affect any of those measurements compared to vehicle. Final group numbers were n=18 vehicle, n=19 1 mg/kg, n=16 3 mg/kg, n=18 10 mg/kg after excluding wild-type animals (n=1 vehicle, n=1 3 mg/kg) and animal death (n=2 1 mg/kg). (j,k) Pancreatic islet analysis and (l) IAPP (soluble and insoluble) levels in pancreas homogenates after 41 weeks of treatment in transgenic rats weekly injected (i.p.) with chα-IAPP-O and vehicle. Representative images (j) and quantitative analysis (k) of transgenic rat islets stained with the beta cell marker insulin (in red) and hIAPP (in green) indicating increased islet area (n=18 for each group; two-tailed unpaired t test: t=2.386, df=34, *P=0.0227), insulin-positive beta cell area (n=18 for each group; two-tailed unpaired t test: % islet area t=1.721, df=34, P=0.0944; % pancreas area t=2.230, df=34, *P=0.0324), hIAPP-positive beta cell area (n=9 10 mg/kg, n=11 vehicle; two-tailed unpaired t test: % islet area t=3.209, df=18, **P=0.0049; % pancreas area t=3.106, df=18, **P=0.0061) and beta cell mass (n=18 for each group; two-tailed unpaired t test: t=2.019, df=34, P=0.0515) in the chα-IAPP-O 10 mg/kg treatment group compared to vehicle (1 and 3 mg/kg groups were not tested). chα-IAPP-O increased soluble IAPP (not statistically significant; one-way ANOVA: F(3,67)=1.300, P=0.2817) and dose-dependently decreased insoluble IAPP in pancreas homogenates (one-way ANOVA: F(3,67)=2.901, P=0.0413; post hoc Dunnett's multiple comparisons test 10 mg/kg versus vehicle: *P=0.0495). Scale bar: 100 μm. All data are expressed as means ± s.e.m.

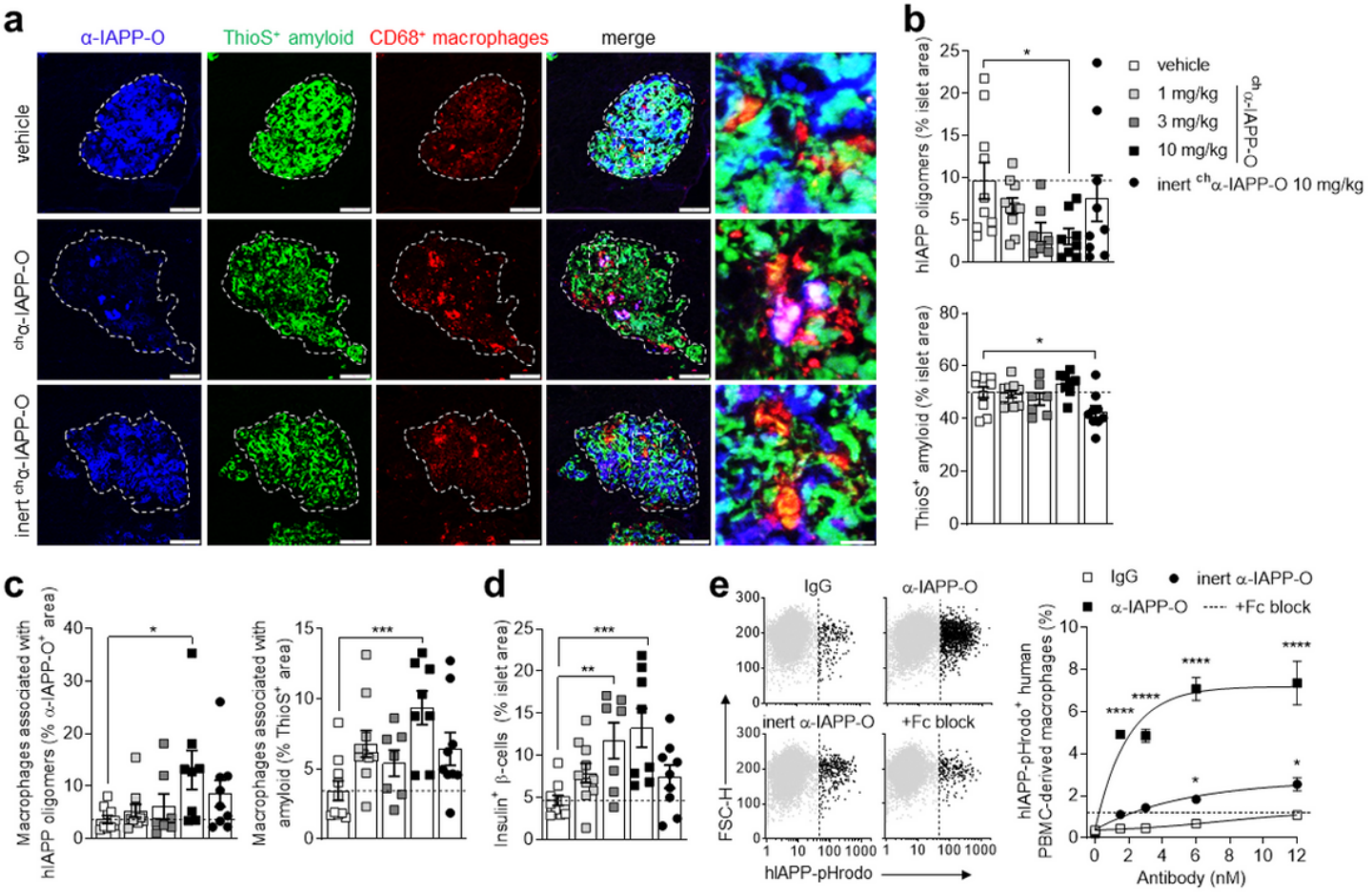

Figure 5

α-IAPP-O stimulates macrophage-dependent clearance of hIAPP oligomers. (a-c) Representative images (a) and quantitative analysis (b-d) of islets from 50-week-old transgenic rats weekly injected (i.p.) with chα-IAPP-O (1 mg/kg, 3 mg/kg, 10 mg/kg), inert chα-IAPP-O (10 mg/kg) and vehicle for 38 weeks. Pancreatic islets were stained for α-IAPP-O-positive oligomers (in blue; three day after i.p. administration of 30 mg/kg α-IAPP-O), ThioS-positive amyloid fibrils (in green) and CD68-positive rat macrophages (in red). Scale bars: 100 and 20 µm. Quantification of hIAPP oligomer and amyloid fibril deposition in relation to islet area (b), and CD68-immunoreactive macrophages associated with these deposits (c). chα-IAPP-O dose-dependently reduced hIAPP oligomers (one-way ANOVA: $F(4,39)=2.269$, $P=0.0791$; post hoc Dunnett's multiple comparisons test 10 mg/kg versus vehicle: *$P=0.0476$, 3 mg/kg versus vehicle: $P=0.0899$) but not amyloid fibrils and increased colocalization of macrophages with both oligomers and fibrils when administered at 10 mg/kg (one-way ANOVA: $F(4,39)=2.732$ and 4.700, $P=0.0426$ and 0.0034; post hoc Dunnett's multiple comparisons test 10 mg/kg versus vehicle: *$P=0.0146$ and ***$P=0.0006$). Islet amyloid load was lower in rats receiving inert chα-IAPP-O 10 mg/kg (one-way ANOVA: $F(4,39)=3.892$, $P=0.0094$; post hoc Dunnett's multiple comparisons test inert chα-IAPP-O 10 mg/kg versus vehicle: *$P=0.0303$). (d) Quantitative analysis of insulin-immunoreactive beta cells in pancreatic islets revealed a dose-dependent increase in beta cell area in transgenic rats receiving chα-IAPP-O treatment compared to vehicle (one-way ANOVA: $F(4,39)=5.258$, $P=0.0017$; post hoc Dunnett's multiple comparisons test 3

mg/kg versus vehicle: **P=0.0090, 10 mg/kg versus vehicle: ***P=0.0008). Final group numbers in a-d were n=10 vehicle, n=10 1 mg/kg, n=7 3 mg/kg, n=8 10 mg/kg chα-IAPP-O, n=9 inert chα-IAPP-O 10 mg/kg after excluding wild-type animals (n=1 3 mg/kg) and animal death (n=2, 3 and 10 mg/kg). (e) Uptake of hIAPP oligomers conjugated to the pH-sensitive dye pHrodo (hIAPP-pHrodo) by PBMC-derived human macrophages in the presence of α-IAPP-O, inert α-IAPP-O and IgG control antibodies at increasing concentrations using flow cytometry. Blocking of Fc receptors expressed on macrophages was used to inhibit phagocytosis induced by α-IAPP-O at 12 nM (+Fc block, represented by a dashed line). Scatterplots of viable singlet macrophages plotted as a function of hIAPP-pHrodo versus forward scatter height (FSC-H) fluorescence intensities, and selection of hIAPP-pHrodo-negative (grey) or -positive (black) populations (left). Dose-response curves (right) showing increased phagocytosis of hIAPP oligomers by macrophages exposed to α-IAPP-O and to a lesser extend inert α-IAPP-O compared to IgG (repeated measures two-way ANOVA (concentration x treatment): F(8,24)=25.84, P<0.0001; post hoc Dunnett's multiple comparisons test α-IAPP-O versus IgG at 1.5, 3, 6 and 12 nM: ****P<0.0001, inert α-IAPP-O versus IgG at 1.5, 3, 6 and 12 nM: P=0.2835, P=0.0850, *P=0.0360 and **P=0.0080). Data are from three biological replicates. All data are expressed as means ± s.e.m.

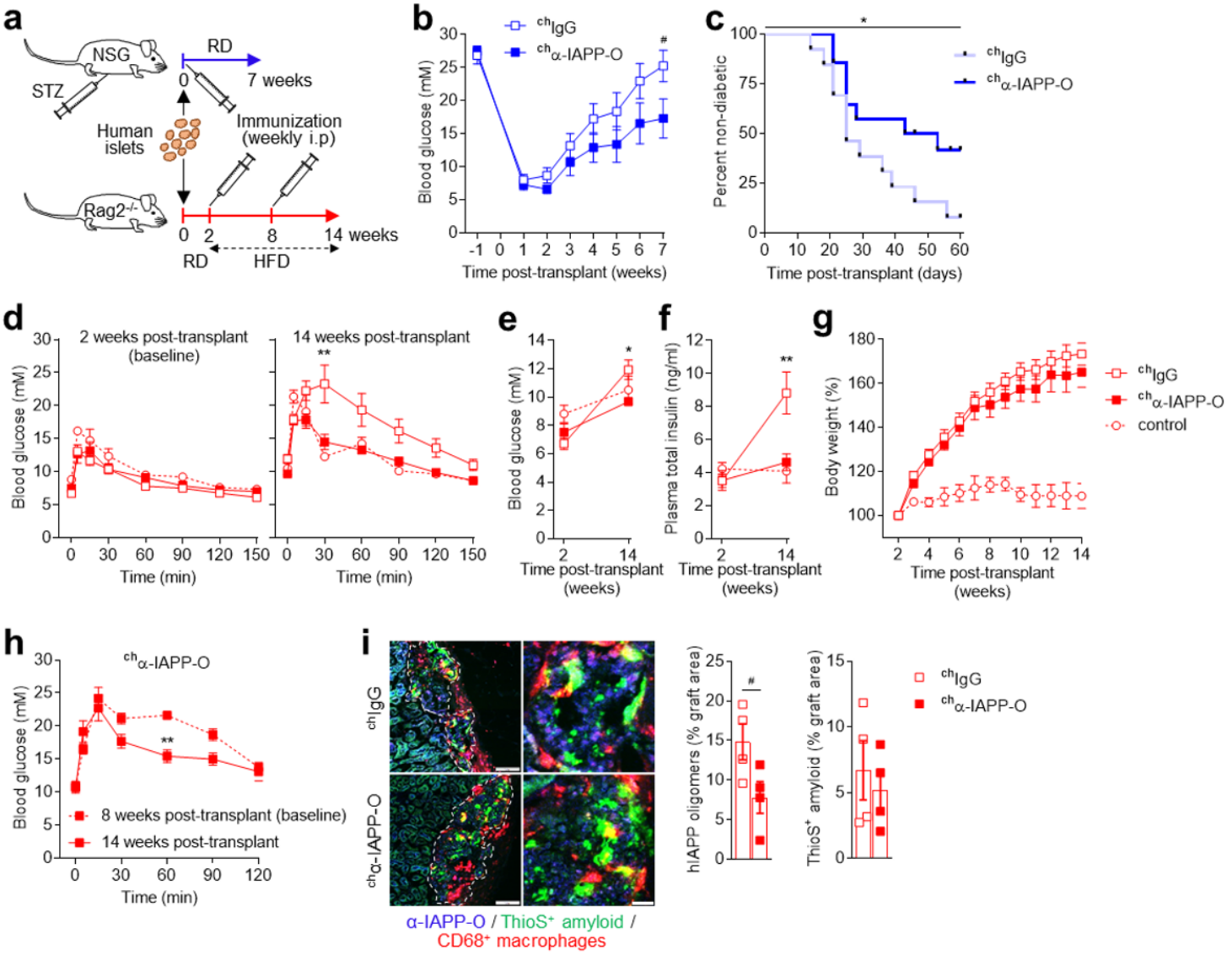

Figure 6

α-IAPP-O improves human islet graft function in diabetic mice. (a) Experimental design to evaluate chα-IAPP-O pharmacological efficacy in human islet-engrafted NSG and Rag2 null mouse models. Human pancreatic islets were transplanted at suboptimal doses under the kidney capsule of streptozotocin (STZ)-induced diabetic NSG mice (b,c) and Rag2 null (Rag2-/-) mice subsequently placed on high-fat diet (HFD) to promote diabetes (d-i). RD, regular diet. (b) Recurrence of hyperglycaemia in NSG recipient mice weekly injected (i.p.) with mouse chimeric α-IAPP-O (chα-IAPP-O, 10 mg/kg) and IgG control (chIgG, 10 mg/kg). Fasting blood glucose values were reduced in mice receiving chα-IAPP-O although not reaching statistical significance (repeated measures two-way ANOVA (time x treatment): $F(7,175)=1.880$, $P=0.0753$; post hoc Sidak's multiple comparisons test chα-IAPP-O versus chIgG 7 weeks post-transplant: #P=0.0595). Blood glucose values represent the average of biweekly measurements. (c) chα-IAPP-O treatment prevents recurrence of diabetes determined by two consecutive fasting blood glucose values above 13 mM (Kaplan-Meier curves of non-diabetic mouse percentage; Log-rank (Mantel-Cox) test chα-IAPP-O versus chIgG: *P=0.0472). Data in b,c are from three independent experiments using human islets preparations from three non-diabetic donors (Supplementary Table 2) and final group numbers were n=13 chIgG and n=14 chα-IAPP-O. (d-f) Blood glucose concentration during oral glucose tolerance tests (d), fasting blood glucose (e) and plasma insulin levels (f) 2 weeks (baseline) and 14 weeks post-transplant in HFD-fed Rag2-/- recipient mice weekly injected (i.p.) with chα-IAPP-O (10 mg/kg) and chIgG control (10 mg/kg) for 12 weeks (14 weeks post-transplant). Naïve Rag2-/- recipient mice kept on regular diet for 12 weeks served as controls. chα-IAPP-O treatment for 12 weeks improved glucose tolerance (repeated measures two-way ANOVA (time x treatment): $F(7,91)=3.741$, $P=0.0013$; post hoc Sidak's multiple comparisons test at 30 min: **P=0.0010), reduced fasting blood glucose (repeated measures two-way ANOVA (time x treatment): $F(1,13)=8.321$, $P=0.0128$; post hoc Sidak's multiple comparisons test: *P=0.0170) and plasma insulin levels (repeated measures two-way ANOVA (time x treatment): $F(1,12)=8.741$, $P=0.0120$; post hoc Sidak's multiple comparisons test: **P=0.0035) compared to chIgG. (g) Body weight of Rag2-/- recipient mice described in d-f expressed as percent increase from baseline. Data in d-g are from two independent experiments using human islets preparations from two pre-diabetic donors (Supplementary Table 2) and final group numbers were n=9 chIgG (n=8 in f), n=6 chα-IAPP-O and n=2 control. (h-i) oGTT blood glucose levels (h) and immunofluorescence analysis of human islet grafts (i) in HFD-induced diabetic Rag2-/- recipient mice weekly injected (i.p.) with chα-IAPP-O (10 mg/kg, n=4) and chIgG (10 mg/kg, n=4) for 6 weeks (8 to 14 weeks post-transplant). Human islets were isolated from a pre-diabetic donor (Supplementary Table 2). (h) chα-IAPP-O treatment improved glucose tolerance (repeated measures two-way ANOVA (time x treatment): $F(6,36)=8.227$, $P<0.0001$; post hoc Sidak's multiple comparisons test at 60 min: **P=0.0028). (i) Representative images and quantitative analysis of human islet grafts stained for α-IAPP-O-positive oligomers (in blue; three day after i.p. administration of 30 mg/kg α-IAPP-O; two-tailed unpaired t test: $t=2.330$, $df=6$, #P=0.0586), ThioS-positive amyloid (in green; two-tailed unpaired t test: $t=0.5591$, $df=6$, $P=0.5963$) and CD68-positive mouse macrophages (in red). Scale bars: 100 and 20 μm. Data are expressed as means ± s.e.m.

Supplementary Files

This is a list of supplementary files associated with this preprint. Click to download.

- SupplementaryInformation.docx